

## REVIEW

[View Article Online](#)  
[View Journal](#) | [View Issue](#)

Cite this: *Mater. Adv.*, 2022, **3**, 7406

Received 30th June 2022,  
Accepted 21st August 2022

DOI: 10.1039/d2ma00793b

[rsc.li/materials-advances](https://rsc.li/materials-advances)

# Stimuli-responsive one-dimensional photonic crystals: design, fabrication and sensing

Marie Däntl,<sup>ab</sup> Alberto Jiménez-Solano<sup>id ad</sup> and Bettina V. Lotsch<sup>id \*abc</sup>

A wide range of sensors, for example in healthcare, electronics or environmental monitoring, have become indispensable parts of our everyday life and smart sensing technologies, fueled by the Internet of Things, are in high demand. However, most sensors rely on a complex readout as they depend on additional electronics and hence the demand for sensors that can be read out optically with a camera or the naked eye has been growing significantly. Photonic crystals (PCs) and related sensing principles are promising candidates as they are responsive to different stimuli and their readout can be achieved optically. In addition, the properties of PCs can be tailored on-demand so as to meet the users' requirements. In this review, we present an overview of the state-of-the-art of stimuli-responsive PC sensors and delineate how stimuli-responsiveness can be created for desired applications based on optical design and nanoscale fabrication.

## 1 Introduction

In the past few decades, especially since the rise of the Internet of Things (IoT), there has been an ever-growing demand for sensors as they have become an integral part of everyday life, and novel applications keep emerging.<sup>1</sup> This is evident from

the increasing number of publications (over half a million) found in an analysis of the Web of Science™ core database for the term “sensor” taking into account the years 2013–2021. There are diverse applications for sensors such as in environmental monitoring,<sup>2,3</sup> food and water control,<sup>4</sup> medical devices,<sup>5</sup> wearables,<sup>6,7</sup> smartphones,<sup>8</sup> or optoelectronics.<sup>9</sup> In particular, gas sensor technologies have attracted great interest (45 770 publications for “gas sensor” from 2013–2021 in the Web of Science™ core database), and the development of new applications leads to new technological challenges and economical requirements. For example, the stability, cyclability, selectivity and sensitivity, quick response, miniaturization, low power consumption, low cost and possibility for wireless

<sup>a</sup> Max Planck Institute for Solid State Research, Heisenbergstrasse 1, 70569 Stuttgart, Germany. E-mail: [b.lotsch@fkf.mpg.de](mailto:b.lotsch@fkf.mpg.de)

<sup>b</sup> Department of Chemistry, Ludwig-Maximilians-Universität (LMU), Butenandtstrasse 5-13, 81377 Munich, Germany

<sup>c</sup> E-conversion, Lichtenbergstrasse 4a, 85748 Garching, Germany

<sup>d</sup> Departamento de Física, Universidad de Córdoba, Edificio Einstein (C2), Campus de Rabanales, 14071 Córdoba, Spain



Marie Däntl

Marie Däntl received her BSc and MSc in chemistry from the LMU Munich in 2015 and 2017, respectively. Since 2018, she carries out her PhD research under the supervision of Bettina V. Lotsch at the Max Planck Institute for Solid State Research. Her research interests include synthesis, assembly and functionalization of nanosheet-based photonic crystals for gas sensing applications.



Alberto Jiménez-Solano

Alberto Jiménez-Solano received his PhD from the University of Sevilla (Spain) in 2017. After his postdoctoral stay at the Max Planck Institute in Stuttgart (Germany), he is currently working as a Distinguished Researcher under the framework of the prestigious Beatriz Galindo program at the University of Córdoba (Spain). His research interests include one-dimensional photonic crystals, optical disordered media and optoelectronic devices.



communication are factors that should be taken into account.<sup>10</sup> Depending on the specific application, different readout and detection principles are favored. The most widely used gas sensing platforms are based on metal oxide semiconductor (MOS)<sup>11</sup> or electrochemical sensors,<sup>12</sup> which make use of changes in the resistance, capacitance or current within the active material upon exposure to a stimulus. Other possibilities include chromatography-based detection, or calorimetric elements, such as catalytic beads, which measure temperature or resistance shifts upon gas adsorption, and acoustic sensors that measure the change in velocity. However, the latter methods tend to be either costly, exhibit low sensitivity, or rely on a complex readout.<sup>13</sup> In contrast, colorimetric sensors, especially when combined with statistical data analysis techniques such as principal component analysis (PCA), are a promising detection platform as they can provide label-free readout without additional wiring due to color changes in response to an external stimulus, which can be detected qualitatively with the naked eye.<sup>14–17</sup> This is evident from the analysis of the number of publications (9796 from 2015–2021) and citations (161 540 from 2015–2021) found for the keyword “colorimetric sensor” in the Web of Science™ core database (see Fig. 1). The implementation of a naked eye readout may play an important role in the progressive miniaturization of sensors, especially for applications regarding the IoT.

Photonic crystals (PCs) are ideal candidates for the fabrication of such colorimetric sensors, as they can be used for gas sensing and the detection of other external stimuli alike.<sup>18–20</sup> They are label-free, can exhibit quick response times, and their fabrication as well as functionalization is facile.<sup>21</sup>

In general, PCs are comprised of two dielectric materials (including air) with different refractive indices (RIs) and show optical band structures characterized by photonic bandgaps. In terms of architectures, PCs can be divided into 1-, 2- or 3D periodic structures according to the dimensionality of their

lattice.<sup>22</sup> Especially one-dimensional photonic crystals (1DPCs), also known as Bragg stacks (BSs), Bragg mirrors or distributed Bragg reflectors (DBRs), which are comprised of two materials with low and high RIs stacked alternately in one spatial direction, are interesting candidates for colorimetric sensing applications. This arises from the fact that the theory and sensing mechanism underlying 1DPCs is particularly straightforward, which enables the prediction of their properties and the rational design to meet the users' requirements.<sup>23</sup> For this reason, our review focuses on 1DPCs. Furthermore, a large library of materials, including nanoparticles, polymers, and nanosheets, has been explored for the fabrication (see Fig. 2) of stimuli-responsive 1DPCs, and their properties can be

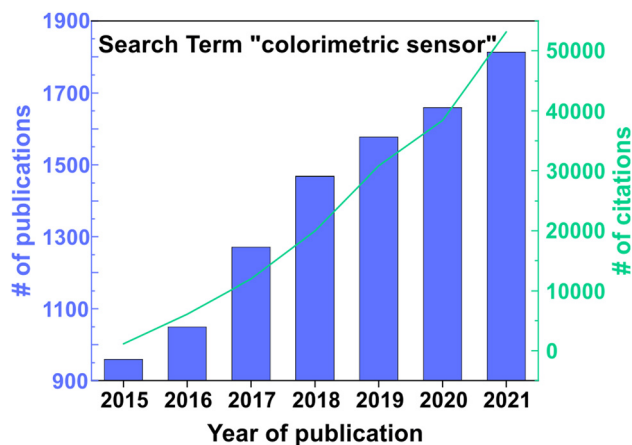


Fig. 1 Number of publications per year (left y-axis) and number of citations per year (right y-axis) for the keyword “colorimetric sensor” in the Web of Science™ core database. Accessed 27.06.2022.



Bettina V. Lotsch

is honorary professor at the LMU Munich and at the University of Stuttgart. In her research, solid-state chemistry, nanochemistry, and molecular chemistry converge for applications in sensing and energy conversion.

Bettina V. Lotsch is the director of the Nanochemistry Department at the Max Planck Institute for Solid State Research in Stuttgart (MPI-FKF). She studied Chemistry at the Ludwig-Maximilians-Universität München (LMU) and the University of Oxford and received her PhD from LMU Munich. After a postdoctoral stay at the University of Toronto she became professor at LMU Munich in 2009 and was appointed Director at MPI-FKF in 2017. She

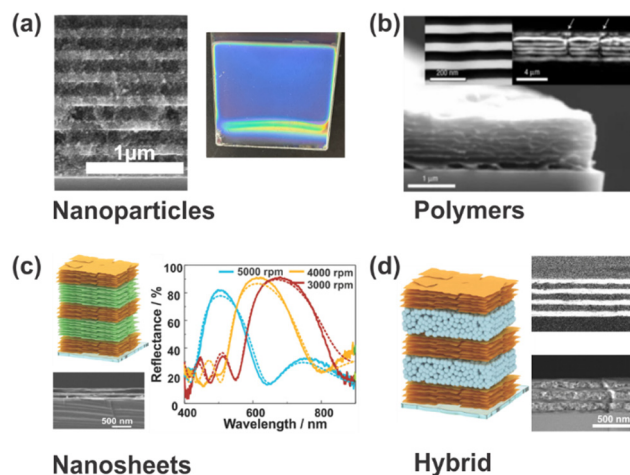


Fig. 2 Different materials used for the fabrication of stimuli-responsive 1DPCs. (a) Inorganic  $\text{TiO}_2$  and  $\text{SiO}_2$  nanoparticles. (b) Polystyrene-*b*-quaternized poly(2-vinyl pyridine) (PS-*b*-QP2VP) polymers; reprinted with permission from ref. 24, Copyright 2007 Springer Nature. (c)  $\text{H}_3\text{Sb}_3\text{P}_2\text{O}_{14}$  and  $\text{Li}_2\text{Sn}_2\text{S}_5$  nanosheets; adapted and reprinted with permission from ref. 25, Copyright 2018 John Wiley and Sons. (d)  $\text{Li}_2\text{Sn}_2\text{S}_5$  nanosheets and  $\text{TiO}_2$  nanoparticles; adapted and reprinted with permission from ref. 25, Copyright 2018 John Wiley and Sons.



rationally tuned by intercalation or inclusion of defects, which makes them a uniquely versatile sensing platform.<sup>18</sup>

In this review, we highlight the research in the field of stimuli-responsive 1DPCs on a conceptual level to showcase the many possibilities regarding their design and application. We do so by presenting basic information on the fabrication of 1DPCs and the materials that can be used, as well as the theoretical concepts underlying their optical properties that allow the design and fine-tuning of stimuli-responsive 1DPCs. Furthermore, we give an overview of the state-of-the-art of stimuli-responsive 1DPCs considering different sensing mechanisms (RI vs. layer thickness change) as well as possible stimuli (physical and chemical). Finally, we discuss selected applications of stimuli-responsive 1DPCs with a focus on vapor and gas sensing as we anticipate that this field has the highest potential for future applications. Before a short outlook, we address the challenges of the sensor performance and how they may be overcome.

## 2 Fabrication of 1DPCs

In this section, we give an overview of the different fabrication approaches that are typically used for creating 1DPCs and compare their advantages and disadvantages.

In general, PCs can be fabricated by top-down as well as bottom-up methods.<sup>26,27</sup> Top-down methods mostly rely on traditional microfabrication tools such as etching to produce microstructures from bulk materials, and are often more controllable than bottom-up techniques. For instance, a 1DPC consisting of porous silicon was fabricated by means of electrochemical etching in acidic medium by controlling the electrical pulse to achieve different levels of porosity in the layers.<sup>28</sup> Further, wet chemical etching was performed to obtain porous GaN structures by removing a sacrificial layer.<sup>29</sup> However, many microfabrication processes require complex instrumentation, which is why microfabricated crystals are not typically used for the preparation of 1DPCs. Due to the experimental ease of bottom-up techniques, we limit our discussion to these approaches with the focus lying on wet deposition methods.

The bottom-up technique is often favored as an efficient and scalable approach that makes use of the assembly of preformed building blocks into periodic photonic structures. Generally, self-assembly is defined as the spontaneous organization of matter, *e.g.* atoms, molecules, colloids or polymers, to a higher level of structural order and complexity by means of non-covalent interactions. This process can be driven by different kinds of weak forces that operate over multiple length scales.<sup>30</sup> So far, the most widely used method for the fabrication of 1DPCs is evaporation-induced self-assembly (EISA).<sup>31</sup> It has been applied, *e.g.*, for the assembly of anisotropic as well as spherical nanocrystals on solid substrates. Particularly, the assembly of the building blocks begins from a homogeneous solution or suspension with a high degree of disorder. When the suspension is spread on a flat and clean substrate (*e.g.*

silicon or glass), evaporation of the solvent in a controlled manner leads to a progressively increasing concentration of the building blocks, which results in the assembly of the building blocks in a preferred orientation at the air/solvent or substrate/solvent interface, thereby forming highly ordered films. The assembly is driven by the fact that the relatively weak attractive forces (*e.g.* van der Waals forces or electrostatic interactions) between the nanocrystals become apparent due to the fact that they come closer to one another with decreasing volume of the solvent.<sup>32</sup>

The easiest form of EISA is the drop-casting method in which a drop of the suspension is placed on a substrate and the sample is left to dry, which induces an assembly of the building blocks at the liquid/air interface during evaporation. With this method, the formation of a film is fast and the process is scalable, but the homogeneity and the control over positioning and alignment of the building blocks is quite low compared to other solvent mediated deposition methods.<sup>33</sup> Especially the edges of the drop-casted film are much thicker than the rest of the sample due to the so-called “coffee ring effect”, which also negatively influences the reproducibility of drop-casted samples.<sup>34,35</sup> Thus, due to its drawbacks, this method is not used frequently for the fabrication of 1DPCs, but is rather applicable for the formation of thin films where thickness control is no primary concern.

Another straightforward solution processing approach for the fabrication of high-quality 1DPCs, which relies on EISA, is the spin-coating method. It has been applied for various systems such as NP suspensions,<sup>36,37</sup> nanosheet suspensions,<sup>25</sup> or polymer solutions.<sup>38</sup> For this process, stable colloidal suspensions with known concentrations are used. It is favorable to prepare the suspensions in a solvent that evaporates quickly, such as alcohols, in order to fabricate homogeneous layers. After deposition of the suspension on a substrate, it is rotated at 2000 to 4000 revolutions per minute (rpm), whereby the majority of the excess material is removed during the acceleration step due to centrifugal forces. The spinning leads to an evaporation of the volatile solvent, which increases the viscosity of the remaining suspension, and the thin film is formed (see Fig. 3). Subsequently a heating step is applied to stabilize the thin film by removing residual solvent. For the formation of multilayer structures, the spin-coating and heating steps are repeated until the desired number of layers is achieved. Since the film thickness can easily be controlled and tuned by variation of the acceleration speed, final rotation speed, concentration of the suspensions or the number of applied deposition steps, the thickness and therefore the properties of 1DPCs can easily be designed and predicted (see Chapter 4). Note that the choice of solvents has to be made carefully to avoid dissolution and penetration between the constituent layers.<sup>39</sup> Major advantages of this method include reproducibility, low cost and a high degree of scalability, as they are compatible with current microfabrication technology.<sup>40</sup> However, the drawbacks are that most of the suspension used for the film-formation is wasted as it is spun off during rotation, and that striating often occurs due to the spinning (see microscope image in Fig. 3).





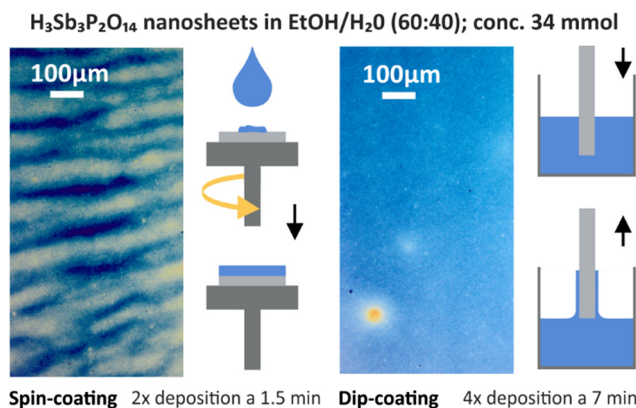


Fig. 3 Comparison of  $\text{H}_3\text{Sb}_3\text{P}_2\text{O}_{14}$  nanosheet-based thin films obtained by spin- (left) and dip-coating (right) including microscope images, the used parameters and schematic descriptions of both processes.

Similar to spin-coating, the dip-coating technique, which is also used in the context of layer-by-layer (LBL) assembly, relies on EISA from stable colloidal suspensions and quick evaporation of the solvent is needed to ensure a homogeneous deposition. It has been applied for various systems such as NP-based 1DPCs,<sup>41–43</sup> or the fabrication of hybrid  $\text{TiO}_2$ /polymer 1DPCs,<sup>44</sup> to name a few. Generally, a substrate is dipped into the suspension (often using an automated dipping system or robot), retrieved with a certain speed and left to dry before the next dip (see Fig. 3). During the drying process, the capillary force-induced meniscus at the interface of the substrate and the dispersion acts as the driving force for the crystallization of the building blocks into a thin film.<sup>45</sup> For the formation of multilayer structures, the dip-coating and drying steps are repeated until the desired number of layers is obtained. Compared to spin-coating, the obtained structures are more homogeneous (see microscope image in Fig. 3) and exhibit less defects, especially at the corners of the sample. Also, striating, which is often observed in spin-coated samples, occurs less frequently. Moreover, dip-coated structures can be assembled on curved surfaces or spheres, unlike spin-coated 1DPCs.<sup>46</sup> By controlling the concentration and viscosity of the suspension, the number of dips or the retrieval speed, the thickness of the resulting 1DPCs can be judiciously designed. However, a rather large amount of suspension in which the substrate can be immersed is required. Moreover, a higher number of dipping steps is often needed to obtain a similar sample thickness compared to the spin-coating technique, and the drying time between the dips is longer than for spin-coated samples. This in turn is time consuming and sedimentation of the particles in the suspension or evaporation of the solvent can occur, resulting in an altered concentration of the suspension. Therefore, depending on the number of fabricated samples, they may not be comparable. Furthermore, the humidity and temperature may also vary over time, which might lead to changes in solvent evaporation or drying times between the dipping steps and hence environmental parameters (temperature, humidity) need to be kept constant during the entire sample fabrication time.

Another bottom-up approach for the fabrication of 1DPCs is the self-assembly of block copolymers, which is based on microphase separation driven by the positive free energy of mixing of the chemically different polymer blocks.<sup>18</sup> Usually the following steps are involved: initially the copolymer precursor solution is spin-coated on a substrate, which is followed by a solvent vapor annealing step. The annealing induces movement of the polymer chains, which leads to the formation of ordered layers.<sup>39</sup> Optional steps are quaternizing and crosslinking of the polymers. For instance, this approach was applied for the fabrication of Polystyrene-*b*-quaternized poly(2-vinyl pyridine) (PS-*b*-QP2VP) PCs.<sup>24</sup> Since this fabrication method is based on the self-assembly of block copolymers, the material choice is obviously limited. Nevertheless, the 1DPCs obtained with this method are highly ordered and can be fabricated in a facile manner.

### 3 Optical properties of photonic crystals

In order to predict and design stimuli-responsive PCs for various sensing applications, it is important to understand their optical properties and sensing mechanism. PCs are nanostructures comprised of periodically arranged dielectric materials with different RIs. In 1987, John and Yablonovitch independently recognized and explored the conceptional analogy between the electronic structure of periodic solids and their dielectric counterparts, making photonic band gap (PBG) materials or PCs the electromagnetic analogue to semiconductor crystals. PCs have the ability to influence the propagation of electromagnetic waves due to the periodicity of their dielectric function, similar to how the motion of electrons is affected by the periodic lattice in semiconductor crystals.<sup>47,48</sup> It was shown that PCs exhibit optical band structures and possess photonic bandgaps, whereby the latter are defined as the frequency ranges in which the propagation of electromagnetic waves is forbidden in certain directions within the structure. The possibility to control the flow of light within PBG materials renders them suitable for various applications such as optical fibers, filters, waveguides, or colorimetric sensors.<sup>49–51</sup>

As mentioned before, PCs can be periodic in 1-, 2- or 3 spatial dimensions (Fig. 4), which influences the resulting dimensionality of their bandgap in reciprocal space.<sup>22</sup>

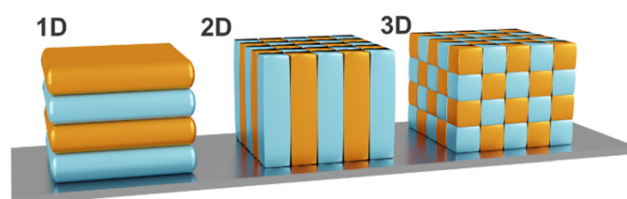


Fig. 4 Schematic representation of 1D, 2D and 3D PCs. Different colors indicate different dielectric constants, exhibiting periodicity in one- (1D), two- (2D) or three-dimensions (3D).



Inspired by photonic nanostructures known from nature such as peacock feathers<sup>52</sup> or butterfly wings,<sup>53</sup> much effort has been directed to creating artificial PCs. The efforts regarding the understanding of the physical theories behind PCs, along with major advances in the fabrication and material development, rapidly transformed this class of materials into a versatile, multifunctional platform for optical sensing. Especially 1DPCs are interesting candidates for colorimetric sensing applications as their fabrication is facile compared to 2D and 3DPCs.<sup>54</sup> Moreover, the properties and sensing mechanism of 1DPCs are easy to predict and hence open up the opportunity to rationally design and control the stimuli-responsiveness of the PCs.<sup>37</sup>

According to eqn (1), a strong interaction of the PC with visible light occurs if the periodicity, *e.g.* the optical thickness  $\tau$  of the material, is in the same range as the wavelength of the light interacting with the PC. Hereby,  $\tau$  is given by the product of the thickness of an individual layer,  $d_l$  or  $d_h$  (for the low or high RI material), and its RI  $n_l$  or  $n_h$ , respectively:<sup>54</sup>

$$\tau_l = n_l \cdot d_l \quad (1)$$

The reflection and diffraction of light impinging on the periodic arrangement of dielectric films in the PC can be described in a similar fashion as the phenomenon of X-ray diffraction: upon propagation of the incident beam through the material, it is partially diffracted and reflected at each interface of layers with different RIs as a function of the optical thickness  $\tau$  of the constituent layers contributing to the bilayer (see Fig. 5) and the angle of incidence (see eqn (2)). Note that the stack of a high and a low RI layer is referred to as a bilayer.

The reflected light beams interfere in a constructive or destructive fashion, which leads to a strong reflectance in a defined wavelength regime, while at the other wavelengths the light is transmitted. The former phenomenon describes the forbidden energy range in which no light waves propagate in the structure along the direction of periodicity.<sup>55</sup> In this range, a reflection maximum occurs, whereas the other spectral

regions exhibit a maximum in transmission. Thus, by periodic stacking of inherently colorless materials, it is possible to achieve a strong color, so called structural color, provided the photonic bandgap lies in the visible region of the spectrum. This phenomenon can be exploited for optical sensing or for the application of PCs as wavelength-selective filters. The central position of the photonic stopband can be derived from the Bragg-Snell laws (eqn (2)):<sup>18</sup>

$$m\lambda_0 = 2D\sqrt{n_{\text{eff}}^2 - \sin^2 \theta} \quad (2)$$

whereby  $m$  is the order of diffraction,  $\lambda_0$  describes the position of the stopband,  $D$  is the lattice parameter with  $D = d_l + d_h$ , where  $d_l$  and  $d_h$  describe the layer thicknesses of the constituent layers of the bilayer,  $n_l$  and  $n_h$  are the corresponding RIs of the constituent layers,  $\theta$  the incidence angle, and  $n_{\text{eff}}$  is the effective refractive index of a bilayer (eqn (3)), defined as:

$$n_{\text{eff}} = \frac{n_l d_l + n_h d_h}{D} \quad (3)$$

It is important to mention that real materials usually show both a spectral dependence of the refractive index as well as a non-negligible imaginary part. Although the latter is negligible in dielectric materials, it becomes more noticeable in metals and semiconductors. Furthermore, the effective refractive index of porous layers is typically described by an effective medium approximation, such as those according to Bruggeman<sup>56</sup> or Maxwell-Garnett,<sup>57</sup> among others.

Additionally, the intensity of the reflectance  $R$  and the bandwidth of the photonic stopband  $\Delta\lambda_0$  can be expressed mathematically according to eqn (4) and (5):

$$R = \left[ \frac{n_0 - n_s \left( \frac{n_l}{n_h} \right)^{2N}}{n_0 + n_s \left( \frac{n_l}{n_h} \right)^{2N}} \right]^2 \quad (4)$$

$$\Delta\lambda_0 = \frac{4\lambda_0}{\pi} \arcsin \left( \frac{n_h - n_l}{n_h + n_l} \right) \quad (5)$$



**Fig. 5** (a) Schematic description of the interaction of light with a 1DPC. The incident beam is partially diffracted at the interfaces between different materials. (b) Calculated model of the influence of the number of bilayers comprising the 1DPC on the optical properties. The RI of the low RI material was  $n_l = 1.2$  for the low and  $n_h = 1.8$  for the high RI material. The number of bilayers was varied from 1 to 6. (c) Calculated model of the influence of the refractive indices of the materials comprising the 1DPC on the optical properties. The low RI was fixed to  $n_l = 1.2$  while the high RI was varied from  $n_h = 1.3$  to  $n_h = 1.8$  in steps of 0.1. The number of bilayers was fixed at 6. Note that (b) and (c) were calculated for a glass substrate with  $n = 1.51$  and a thickness of 1 mm.



whereby  $n_0$  and  $n_s$  describe the RI of the surrounding medium and the substrate,  $N$  is the number of bilayers in the multilayer structure, and  $n_l$  and  $n_h$  correspond to the RIs of the low and high refractive index material.<sup>18</sup>

Fig. 5 gives an overview of the effect of eqn (2), (4) and (5) on the stopband position and width. An increasing number of bilayers leads to a higher reflectance and a narrowed stopband, while an increase of the RI contrast leads to a higher reflectance as well, but a significant broadening of the bandwidth is observed. Furthermore, by changing the layer thickness, a shift of the stopband position is induced, which is represented in Fig. 6.

Considering the above relations, it is evident that the photonic bandgap properties are dependent on the properties of the constituent materials as well as the architecture of the Bragg stack and the properties of the surrounding medium.

## 4 Sensing mechanisms in stimuli-responsive photonic crystals

Based on the photonic architectures and physical principles described above, it is possible to create stimuli-responsiveness in PCs. This opens up the opportunity of using PCs for colorimetric sensing if exposure towards a stimulus leads to an altered diffraction wavelength or intensity. Regarding eqn (1), changes in the structural color of the 1DPC occur if a stimulus leads to changes in the RI or the thickness of the constituent layers (Fig. 6), or both. In most cases, a combination of both possibilities occurs, whereby one of them is predominant for the sensing mechanism. However, the relative change in layer thickness is often more significant than the change in RI, because the RI of a material can only be varied by a small margin in response to external stimuli, while layer thickness changes are less restricted.

Generally, several sensing mechanisms have been observed in stimuli-responsive 1DPCs. The first two options are based on the response to a stimulus either through pore filling or through swelling of the active material. Typically, these two

sensing mechanisms rely on the use of inherently responsive building blocks. Another possible sensing mechanism is based on the inclusion of a responsive “defect layer” in the 1DPC. In the following, we focus on the conceptual overview of the different types of sensing mechanisms in 1DPCs, along with examples of applicable materials.

### 4.1 Sensing through pore filling

In the case of sensing through pore filling, the porosity of the applied 1DPCs can be due to inherent structural porosity of the constituent material, template-induced porosity, or textural porosity. In sensing devices built from porous 1DPCs, the RI is altered upon pore filling through the analyte while the thickness is kept constant, which in turn leads to an optical response of the sensor (Fig. 6a). The first porous BS to be reported in this field was the “smart dust” discovered by Sailor *et al.* in 2003.<sup>58</sup> In this work, two discrete porous multilayered dielectric mirrors were fabricated into silicon through electrochemical etching. One of the mirrors was chemically modified through silane chemistry to exhibit hydrophobic properties, while the other one had hydrophilic properties and both mirrors were designed to have a different optical reflectance. Upon exposure to an analyte, these BSs aligned themselves based on the hydrophilic/hydrophobic properties of the analyte. The subsequent infiltration of the responsive side of the 1DPC leads to a change of the RI and therefore predictable shifts of the optical reflectance are induced.

In 2006 Ozin and co-workers transferred the concept of porous layers for RI sensing to 1DPCs based on mesoporous, sol-gel-derived  $\text{TiO}_2$  and  $\text{SiO}_2$  layers. The authors demonstrated the optical response of this BS upon infiltration with organic solvents having different RIs such as alcohols and alkanes.<sup>59</sup> The next generation of 1DPCs used for RI sensing was based on  $\text{TiO}_2$  and  $\text{SiO}_2$  nanoparticles, leading to textural mesoporosity. These 1DPCs exhibited a response towards volatile organic solvents (VOCs) instead of liquid analytes.<sup>60</sup> Furthermore, porous  $\text{TiO}_2$  and  $\text{SiO}_2$  1DPCs were attached to a flat gold film to induce a sharp Tamm mode within the stopband of the PC.<sup>61</sup>

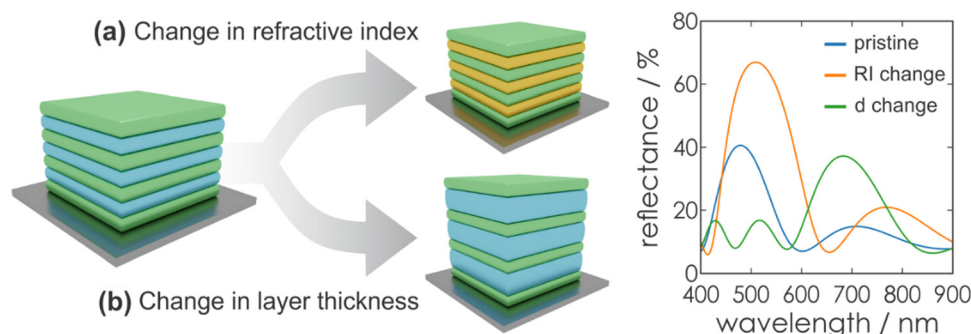


**Fig. 6** Schematic illustration of the possible sensing mechanisms in a 1DPC. Upon exposure towards an analyte either the refractive index change (top) or the layer thickness change (bottom) is predominant. (a) Calculated red-shift of the Bragg peak (orange graph) induced by a change in the RI upon exposure towards a stimulus. The low RI was fixed to  $n_l = 1.6$  while the high RI was changed from  $n_h = 1.8$  to  $n_h = 2.0$ . The thickness of each layer was 70 nm. (b) Calculated red-shift of the Bragg peak (green graph) induced by a change in the layer thickness upon exposure towards a stimulus. The low RI was fixed to  $n_l = 1.6$  and the high RI was fixed to  $n_h = 1.8$  while the layer thickness of the high RI material was changed from 70 to 140 nm. Note that the reflectance spectra in (a) and (b) were calculated for a glass substrate with  $n = 1.51$  and a thickness of 1 mm.



Tamm plasmons are electromagnetic modes confined at the interface between a noble metal layer and the 1DPC, which lead to a dip in the photonic bandgap. Therefore, changes in the refractive index inside the porous structure induced by the exposure to solvents can be probed as the spectral position of the Tamm mode changes in a precise manner.

Apart from NPs other porous, responsive building blocks such as metal-organic frameworks (MOFs)<sup>62,63</sup> or zeolites<sup>64</sup> have been used for creating stimuli-responsive 1DPCs based on a change of the RI. Since the discovery of the stimuli-responsiveness of porous 1DPCs, many efforts in this research field have been conducted, and nowadays these PCs are used in diverse applications ranging from vapor/solvent sensing,<sup>65,66</sup> to sensing of biologically relevant analytes<sup>67,68</sup> to environmental sensing<sup>3</sup> or water and food quality<sup>4,69</sup> control.

Even though a large number of functional NPs and other porous materials is available for creating responsive 1DPCs, and these sensing devices possess a high molecular selectivity, it is important to note that the sensitivity is often low. This drawback is due to the intrinsically limited RI changes upon analyte infiltration, which translate to a rather small stopband shift according to eqn (2). Therefore, materials that rely on a layer thickness change (shrinking or swelling) as sensing mechanism, such as swellable polymers, are beneficial for higher sensitivity and an increased resolution (see Fig. 6).

## 4.2 Sensing through swelling

Swelling in a 1DPC (Fig. 6b) was first reported in 2007 by Kang *et al.* using a PC comprised of polymer layers as stimuli-responsive component and infiltration with a liquid analyte lead to a full-spectral stopband shift (from 364 to 1627 nm).<sup>24</sup> Additionally, a broad solvent and solvent mixture response<sup>70</sup> as well as humidity<sup>71</sup> and chloroform vapor sensitivity<sup>72</sup> has been demonstrated in polymer-based organic-inorganic hybrid 1DPCs, highlighting their wide range of applications. As the polymers possess various functional groups, their responsiveness can be tuned to different external stimuli, making them a versatile sensing platform. Even though the fabrication of polymer based 1DPCs (Fig. 2b) is facile and the library of possible materials<sup>24,71,73,74</sup> is large, the main disadvantages

for polymer based 1DPC sensors are their low RI contrast, slow response and recovery times towards stimuli, and low chemical and long-term stability.

To overcome these drawbacks, the use of 2D inorganic materials (nanosheets) as building blocks for stimuli-responsive 1DPCs has been explored as they exhibit short response and recovery times to external stimuli by taking up analytes between their layers, leading to layer swelling. Compared to polymers, they are more stable, and there is a large diversity in composition and structure. Like for polymers, it is possible to tailor their properties in order to design their responsiveness. The nanosheets that have been applied in stimuli-responsive 1DPCs include antimony phosphates,<sup>75–77</sup> lithium tin sulfide (Fig. 2c),<sup>25</sup> graphene oxide,<sup>78,79</sup> layered double hydroxides,<sup>80</sup> and clays,<sup>81,82</sup> which cover different RIs and therefore allow the fabrication of 1DPCs with a large optical contrast to the other constituent material. Considering that a large RI contrast is beneficial for stimuli-responsiveness, it is desirable to fabricate hybrid (in terms of types of materials, *e.g.* nanosheet/nanoparticle or nanoparticle/polymer) 1DPCs (Fig. 2d), based on either the sensing mechanism (RI *vs.* swelling materials) or the inorganic/organic nature of the materials.

A further approach to prepare swellable 1DPCs has combined the breathing capability of porous MOF nanoparticles (MIL-88B) with their high chemical selectivity for different VOCs, resulting in large stopband shifts as a function of the analyte (see Chapter 7).<sup>83</sup>

## 4.3 Sensing based on the inclusion of a stimuli-responsive defect layer

Another option to exploit the sensing capability of responsive 1DPCs is the inclusion of a “defect layer” with a different optical thickness and responsive properties into the otherwise periodic bilayer structure of 1DPCs in order to induce the tuneability of the photonic bandgap. In this case, the defect layer breaks the periodicity and shifts the position of the allowed state into the original forbidden bandgap.<sup>22</sup> Therefore, a well-defined dip (pass-band) of the reflectance (Fig. 7 blue graph) occurs in the photonic stopband, whereby the position

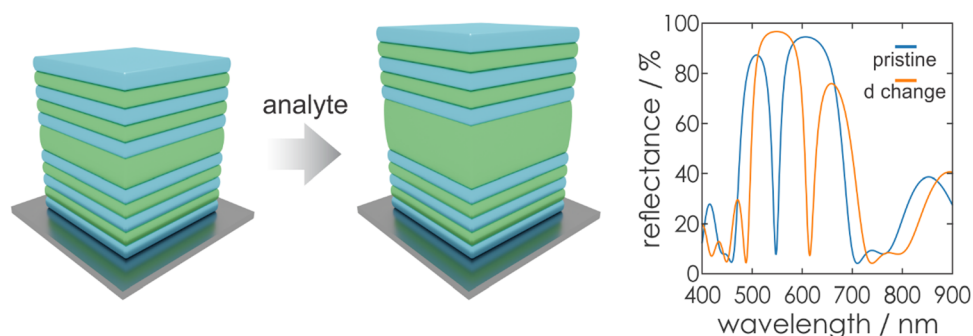


**Fig. 7** Left: Schematic illustration of a defect layer embedded in a 1DPC. Right: Calculated resulting drop in the reflectance caused by the defect in a 1DPC. The RI of the low RI material was  $n_l = 1.5$  and  $n_h = 2.0$  for the high RI material and the defect was embedded in the middle ( $n = 1.5$ ,  $d = 160$  nm) of the 6 bilayers comprising the 1DPC. After analyte exposure the thickness of the defect layer was 240 nm. Note that the reflectance was calculated for a glass substrate with  $n = 1.51$  and a thickness of 1mm. The thickness of each layer in the 1DPC was 80 nm.





and intensity of this transmission maximum is dependent on the optical thickness of the defect layer. Exposure towards a stimulus alters the thickness or RI of the 1DPC, which leads to a shift of the defect state within the bandgap (Fig. 7 orange graph). Since the pass-band is sharp compared to the broad stopband, the analyte resolution of the sensor is very high, and hence even subtle changes in the environment can be detected reliably.<sup>84</sup>

As many different responsive materials are available as defect layers, such as dyes,<sup>85</sup> metallic particles,<sup>86</sup> MOFs<sup>87</sup> or nanophosphors,<sup>88</sup> the possibilities for manipulating the properties of the PC are vast. Additionally, defect layers in 1DPCs can also be achieved by the inclusion of a thicker layer of one of the constituent stimuli-responsive materials, which has been demonstrated for TiO<sub>2</sub>/SiO<sub>2</sub>, graphene oxide hydrogel and TiO<sub>2</sub><sup>89</sup> as well as clay and TiO<sub>2</sub>/SiO<sub>2</sub><sup>82</sup> PCs, among others. Please note that more detailed examples of defect layers in 1DPCs and their application for vapor sensing are given in Chapter 7 and Fig. 11.

## 5 Types of stimuli

In the past few years, the research interest in exploiting structural color for sensing applications has increased, and many stimuli-responsive 1DPCs have been applied as label-free sensing platforms. Generally, 1DPCs can be responsive to various stimuli of physical, chemical or biological nature, which induce a RI or thickness change of the responsive building block and lead to a shift of the photonic stopband. In contrast to the previous chapter, which was mainly focused on the different sensing mechanisms, the following subsections intend to give conceptual insights into the broad variety of different stimuli that 1DPCs can be responsive to. These will be briefly discussed along with a small selection of examples. For a broader overview of literature examples for each stimulus, the reader is referred to other reviews.<sup>18,39,90</sup>

### 5.1 Response to physical stimuli

One of the application fields of stimuli-responsive 1DPCs lies in the detection of physical stimuli, such as mechanical, thermal or electrical stimuli. In the following subsections, we will discuss the different physical stimuli along with some examples to explain the underlying sensing principle.

**5.1.1 Mechanical stimuli.** Mechanical stress, such as compression or stretching, is the simplest type of stimulus 1DPCs are responsive to. In 2006 the group of Ozin was the first to discover that elastomeric inverse opals (3DPCs) can be applied as mechanochromic sensors.<sup>94</sup> Because of the highly porous nature of the elastic inverse opal, it can easily be compressed changing the layer spacing between the air voids. This results in a gradual shift of the photonic stopband across the entire visible spectrum with increasing pressure. This work sparked the interest in using elastic polymers as building blocks for creating mechanically responsive 1DPCs. Generally, mechanical deformation is accompanied with a biaxial contraction/

expansion of the polymer matrix along perpendicular directions in order to maintain a constant volume.<sup>95</sup> This causes changes in the RI or the lattice dimensions and therefore a shift of the photonic stopband is induced. For example, Steiner *et al.* demonstrated that a PC comprised of polymethylsiloxane (PDMS) and PSPI (tri-block copolymer which consists of polyisoprene containing a 22 wt% minority polystyrene phase) exhibits a reduction in layer thickness upon stretching, and therefore the photonic stopband is blue-shifted and can be tuned across the entire visible spectrum (from *ca.* 550 to 670 nm) as a function of the amount of strain (Fig. 8a).<sup>91</sup> Another mechanochromic sensor, based on a polystyrene-*b*-poly-2-vinylpyridine (PS-*b*-P2VP) di-block copolymer, was reported by Stafford and co-workers and exhibited a stopband shift from 760 to 520 nm under compressive strain from 10 to 30%.<sup>96</sup> Additionally, the sensor was cast into conformal coatings on nonplanar or patterned surfaces while maintaining its sensing functionality, making the application possibilities versatile. Even though the deformation and accompanied shift of the photonic stopband in mechanochromic 1DPCs is usually reversible, the long-term stability is poor and the recovery time can be comparatively long. Furthermore, the wavelength tuning range of mechanically responsive 1DPCs is dependent on the volume fraction of the polymer content and the stretching ratio ( $L/L_0$ ). Therefore, it is necessary to fabricate “soft” photonic crystals (with high polymer content) as they exhibit a large stopband shift (*i.e.* large response) under mechanical deformation.<sup>18</sup>

**5.1.2 Thermal stimuli.** A change in the environmental conditions, such as a temperature change, can lead to swelling or de-swelling of 1DPCs. Therefore, the use of hydrogels, which can undergo a volume phase transition in an aqueous environment, is highly beneficial for colorimetric 1DPC temperature sensors. One of the most popular examples is the “smart” polymer poly(*N*-isopropylacrylamide) (PNIPAM), which exhibits a sharp volume phase transition around the lower critical solution temperature (LCST; *ca.* 32 °C). This means that the PNIPAM gel swells when the temperature is below the LCST and undergoes a dramatic collapse when the temperature is above the LCST.<sup>97</sup> The collapse is due to the fact that for temperatures above the LCST a transition from the hydrated (swelled) to the dehydrated (deswelled) state occurs, and thereby the hydrogel properties change from hydrophilic to hydrophobic.<sup>98</sup> For instance, this principle has been exploited for the fabrication of 1DPCs based on the photo-crosslinkable copolymers PNIPAM and poly(*para*-methyl styrene) (PpMS), which exhibit a color change that covers nearly the full visible spectrum when changing the temperature from 20 to 50 °C.<sup>99</sup> This was achieved by immersion of the sensors in water at room temperature, which leads to swelling of the PNIPAM layers and therefore a red-shift of the reflectance. Subsequent heating induced a de-swelling of the layers due to a dramatic collapse as the temperature is increased towards the lower critical solution temperature (LCST), causing a progressive blue-shift of the stopband.

Guan *et al.* also made use of the volume phase transition of PNIPAM with respect to the surrounding temperature.





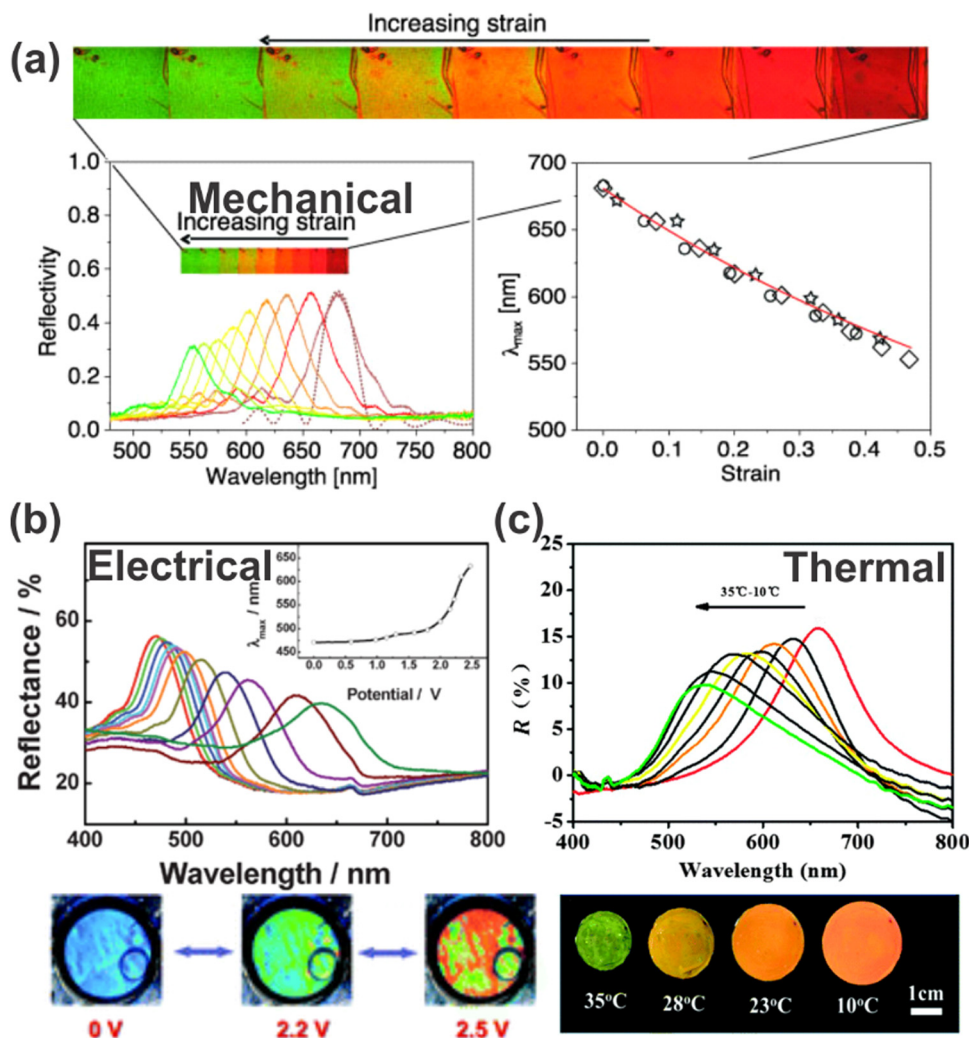


**Fig. 8** Response of 1DPCs to different physical stimuli: (a) reversible color change induced by stretching of a 1DPC; reprinted with permission from ref. 91, Copyright 2010 Optical Society of America. (b) Reflectance spectra and photographs of electrical tuning of a 1DPC; reprinted with permission from ref. 92, Copyright 2009 Royal Society of Chemistry. (c) Reflectance spectra and photographs of a 1DPC with varying temperature; reprinted with permission from ref. 93, Copyright 2015 Royal Society of Chemistry.

They applied this approach for a 1DPC comprised of super-paramagnetic polyvinylpyrrolidone-coated  $\text{Fe}_3\text{O}_4$  colloidal nanocrystalline particles ( $\text{Fe}_3\text{O}_4\text{@PVP CNC}$ ), which order into 1D chains when applying an external magnetic field and can be fixed and solidified in a PNIPAM gel matrix (Fig. 8c).<sup>93</sup> Due to the high RI contrast of the constituent materials, the 1DPC exhibits a bright iridescent color. During a decrease in temperature from 35 to 10 °C, the volume of the gel expands gradually and the color changes from green over yellow and orange to red. This is due to the fact that the gel matrix transforms from hydrophobic to hydrophilic with decreasing temperature, which leads to significantly increased water absorption capabilities. Therefore, a swelling of the matrix is induced, accompanied by a change in the RI and a shift of the stopband from 660 nm to 520 nm.

**5.1.3 Electrical stimuli.** Another type of physical stimulus, which 1DPCs are responsive to, is an electric field. In general, electrically responsive 1DPCs can either be stimulated by an

electrical signal or respond to an electrochemical signal. So far, most of the research in this field has been conducted with 3D photonic crystals while the number of examples for electrically tunable 1DPCs is relatively small. This may be a consequence of the lack of connectivity within the stimuli-responsive material and hence the lack of electric addressability due to the 1D architecture. Nevertheless, we highlight two examples here. One possibility for electrically responsive 1DPCs is achieved when including nematic liquid crystals as a defect layer in an  $\text{SiO}_2$  and  $\text{TiO}_2$ -based photonic structure.<sup>100</sup> When an electric field is applied, the pass-band, which is caused by the defect layer, is shifted as the RI is changed due to the realignment of the liquid crystals in response to external electric fields.

Another possibility for electrically responsive 1DPCs is the response towards electrochemical signals. Examples of electrochemically responsive 1DPCs are based on the block copolymer polystyrene-*b*-poly(2-vinyl pyridine) (PS-*b*-P2VP), which exhibits swelling when an applied electric field changes the chemical



environment, and therefore a full color shift of the photonic stopband is induced (Fig. 8b).<sup>92,101</sup> Precisely, the pyridine group in the P2VP block can be protonated in solution by applying an anodic bias voltage. The resulting pyridinium groups pair with the anions of the electrolyte, which in turn are attracted to the positively charged electrode. Likewise, the reverse process occurs when applying a cathodic bias voltage. These processes enable electrical tuning of the thickness of the PV2P layers or the periodicity of the film as the application of a small voltage leads to an expansion or contraction of the layers as a function of the direction and strength of the electrical potential.

## 5.2 Response to chemical stimuli

Another multifaceted application of stimuli-responsive 1DPCs is the detection of chemical stimuli. These can be liquids, vapors, humidity, pH ( $H^+$  ions) of the surrounding medium, or biomolecules. In the following subsections, we give an overview of different chemical stimuli by discussing some examples to explain the underlying sensing principle and to highlight the vast variety of possible stimuli.

**5.2.1 Solvents, liquids and vapors.** So far, much effort has been devoted to solvent, liquid and vapor sensing due to the quick and large response as well as facile readout of the 1DPCs. A large library of active components, such as porous nanoparticles,<sup>60,65</sup> nanosheets,<sup>25,75</sup> polymers,<sup>24,105</sup> clays,<sup>81,106</sup> MOFs<sup>63</sup> or zeolites<sup>107</sup> has been explored and diverse liquids, organic solvents, VOCs or humidity (Fig. 9a) have been applied as analytes. Depending on the active component used, the sensing principle predominantly relies on RI or thickness changes, which translates into a shift of the photonic stopband. Furthermore, the 1DPCs can function as a “photonic nose” by creating an array of PCs, in which each component is functionalized to respond to a different analyte.<sup>67</sup> The applications for this class of responsive 1DPCs are widespread and range from environmental monitoring,<sup>102</sup> *via* water and food quality control<sup>4</sup> to medical diagnostics.<sup>67</sup> To our mind the field of vapor sensing is highly promising for future applications and should further be investigated. Therefore, a more detailed

discussion of selected examples of 1DPCs used for vapor sensing is given in Chapter 7, which is why we keep the discussion short at this point.

**5.2.2 Ions.** Another possibility for chemical responsiveness of 1DPCs is the response towards pH or ions. Ion responsiveness in 1DPCs is commonly based on the interaction of analyte ions with a certain recognition group of a hydrogel polymer leading to an altered Donnan osmotic pressure.<sup>18</sup> Therefore, a volume change of the hydrogel takes place, which is driven by solvent influx in order to compensate the osmotic pressure.<sup>103</sup> Since this process leads to a swelling or shrinking of the polymer component, a shift of the photonic stopband is induced. For example, Ge and co-workers demonstrated pH-responsiveness in the range from 8 to 2 at a temperature of 35 °C (Fig. 9b) by incorporating a proton-sensitive co-polymer such as poly(acrylic acid-*N,N'*-methylene-bis-acrylamide-*N*-isopropylacrylamide) P(AA-bis-NIPAAm) as active material in a 1DPC.<sup>103</sup> Upon solvent influx, the uptake of  $H^+$  results in electrostatic repulsion in the polymer. The more water infiltrates the 1DPC, the lower the RI of the swollen polymer, leading to a shift in PBG from 575 nm to 510 nm. From the reflectance spectra, it seems that all tested pH values can be distinguished in a proper manner except for pH 6 and 7, which show similar stopband positions.

Another example of ion detection with polymer-based 1DPCs is the use of a polydimethylaminoethyl methacrylate-*co*-ethylene glycol dimethacrylate (PDMAEMA-*co*-PEGDMA) and  $TiO_2$ -based BS, which is responsive to thiocyanate anions ( $SCN^-$ ). Immersion in citric acid leads to a red-shift of the stopband due to swelling of the quaternized polymer and the decrease of its RI. Upon exposure towards  $SCN^-$  (concentrations from  $10^{-6}$  mol  $l^{-1}$  to  $10^{-1}$  mol  $l^{-1}$ ) a blue-shift of the PBG is observed (750 nm to 490 nm) caused by a volume collapse due to weakened electrostatic repulsion in the polymer layers.<sup>39,108</sup> Further, the sensor exhibits a high selectivity towards the detection of  $SCN^-$  as the assay is barely influenced by the presence of other, interfering anions ( $F^-$ ,  $Cl^-$ ,  $Br^-$ ,  $I^-$ ,  $HPO_4^{2-}$ ,  $Ac^-$  and  $HCO_3^-$ ). Despite the fact that there are various other possibilities for sensing ions or



**Fig. 9** Response of 1DPCs to different chemical stimuli: (a) relative humidity; adapted and reprinted with permission from ref. 102, Copyright 2011 American Chemical Society. (b)  $H^+$  ions; adapted and reprinted with permission from ref. 103, Copyright 2015 Elsevier. (c) Glucose oxidase ( $GO_x$ ); adapted and reprinted with permission from ref. 104, Copyright 2012 Royal Society of Chemistry.

pH, stimuli-responsive 1DPCs may offer a platform for miniaturized sensors for specific applications.

**5.2.3 Biomolecules.** Even though most biomolecules are too large to be reasonably detected by 1DPCs, we discuss a few examples in this subsection that show that chemically responsive 1DPCs can also be designed to detect biologically relevant molecules. This is achieved either directly by including an appropriate recognition group into the structure, or indirectly *via* changes in the environment such as the pH, triggered by the interaction of the analyte with the photonic structure. For example, the catalytic oxidation of glucose in the presence of glucose oxidase ( $\text{GO}_x$ ) can be monitored as pH changes occur due to the gluconic acid, which is generated during the reaction. 1DPCs based on poly(*N,N'*-dimethylaminoethyl methacrylate) (PDMAEMA) and  $\text{TiO}_2$  are able to detect the concentration of  $\text{GO}_x$ , since the polymer is pH-sensitive and shrinks or swells in response to the produced gluconic acid, and hence leads to a shift of the photonic bandgap (Fig. 9c).<sup>104</sup> Furthermore, surface functionalization of mesoporous 1DPCs based on  $\text{TiO}_2$ - and  $\text{SiO}_2$ -nanoparticles with biotin allows for the optical detection of probe-target interactions with streptavidin, whereby the response relies on the change in the dielectric constant due to the bio-recognition event. Interestingly, confocal fluorescence microscopy has shown that the streptavidin diffused to deeper layers of the mesoporous 1DPC instead of staying on the surface. Therefore, future research should focus on the diffusion of molecules within 1DPCs in order to gain a deeper knowledge on how to exploit stimuli-responsive 1DPCs for an even wider range of applications.

## 6 Selected vapor sensing applications

In the previous chapters, the various types of stimuli that can be detected with 1DPCs have been discussed on a conceptual level. Since vapor sensing is one of the largest application fields of stimuli-responsive 1DPCs and has received increasing attention in the past few years, the next section focuses on this stimulus in more detail by reviewing selected examples. To structure this discussion, the examples of vapor-responsive 1DPCs are grouped by their architecture being either nanoparticle-based PCs, defect structures, or hybrid photonic structures.

### 6.1 NP-based 1DPCs

For porous nanoparticle-based 1DPCs, which are often comprised of  $\text{SiO}_2$  and  $\text{TiO}_2$  particles, the vapor sensing capabilities regarding humidity,<sup>66,102,109</sup> toluene<sup>60,109</sup> and isopropanol<sup>66,110,111</sup> have been studied. The main reasons for the popularity of this system is its inexpensive and easy fabrication as well as the broad tunability of the optical properties deriving from properties on the macroscopic, mesoscopic and atomic scale.<sup>109</sup> Therefore, the optical response towards environmental changes can be precisely tailored to meet the desired application. These types of 1DPCs are not only sensitive to a certain vapor, but they can also distinguish specific relative vapor pressures of the analyte.<sup>60,66,111</sup> For example, this was studied by Kobler *et al.* for 1DPCs based on mesoporous  $\text{SiO}_2$  and  $\text{TiO}_2$  nanoparticles that exhibit a response towards different vapor pressures of toluene due to changes in the RI, which gives rise to optical adsorption isotherms.<sup>60</sup>

Some 1DPCs are not only stimuli-responsive, but their responsiveness can be changed and fine-tuned by post-synthetic functionalization or intercalation. For example, it has been shown that porous 1DPCs based on alternating layers of  $\text{SiO}_2$  and  $\text{TiO}_2$  NPs can be employed as “artificial nose” for the detection of bacteria, which are commonly involved in cases of opportunistic hospital infections.<sup>67</sup> Bonifacio *et al.* demonstrated that surface functionalized 1DPC sensor arrays, combined with color image analysis, could be used to identify different bacterial strains (*Pseudomonas aeruginosa*, *Escherichia coli*, *Staphylococcus aureus*, and *Staphylococcus epidermidis*) by analyzing the headspace created by them (Fig. 10). When cultivated in 5% sheep blood agar for 24 h, each bacteria strain produces a unique composition of volatile species. Even though the amount of volatiles produced by the bacteria is small, the culture headspace shows a distinct atmosphere composition, which is made up of agar volatiles along with the bacteria culture by-products, and therefore enables the unambiguous distinction of the different bacteria strains. The volatile metabolites of bacteria strains can contain alcohols, sulfides, amines, and aldehydes, among others. A detailed study on the composition of the headspace of some bacteria strains can be found elsewhere.<sup>112</sup> Due to the differently functionalized sensors in the array, the headspace of the studied bacteria strains can be distinguished by PCA analysis. Even though there are many examples of nanoparticle-based



Fig. 10 Principal component analysis of color changes resulting from the exposure of a 1DPC-based photonic-nose array to different analyte-saturated atmospheres (middle) as well as color changes caused by the volatiles produced by bacteria strains (right); adapted and reprinted with permission from ref. 67, Copyright 2010 John Wiley and Sons.





1DPCs used for vapor sensing, the relative optical shift of the stopband of these 1DPCs is intrinsically limited as the optical response relies mainly on the change of RI upon analyte infiltration. It is thus key to implement suitable image or multivariate analysis to discriminate chemically similar analytes in a sufficient manner.

## 6.2 Defect 1DPCs

In order to overcome the drawbacks of nanoparticle-based 1DPCs, the inclusion of a defect layer or the fabrication of hybrid 1DPCs to increase the resolution has received attention in the past few years. Exemplarily, analytes reported for defect 1DPCs range from protic (*e.g.* humidity,<sup>85</sup> ethanol (Fig. 11a),<sup>87</sup> isopropanol<sup>66,88</sup>) to aprotic solvent vapors such as toluene.<sup>88</sup> The underlying sensing mechanism of defect 1DPCs was discussed in more detail in Section 5.3. As mentioned previously, one possibility for defect layers is the fabrication of a thicker layer of one of the constituent materials in the middle of the

1DPC in order to break its symmetry. This approach was utilized by the group of Miguez for the fabrication of a mesoporous  $\text{TiO}_2$ - and  $\text{SiO}_2$ -based 1DPC in which a five times thicker  $\text{SiO}_2$  layer was embedded in the middle of the otherwise periodic photonic structure (Fig. 11a).<sup>66</sup> In their work they gave a detailed analysis of the response of such a defect 1DPC towards isopropanol (Fig. 11a left) and water (Fig. 11a right) vapors with partial pressures from 0 to 1 along with the comparison of the response of the 1DPC without the defect layer. In accordance with the theoretical details discussed in Section 5.3, it is evident that the resolution of the defect-containing PC is higher due to the thin reflectance dip compared to the broad stopband of the normal 1DPC.

Another option for creating defect 1DPCs is the inclusion of other responsive materials such as nanosheets, dyes or nanophosphors (Fig. 11b and c).<sup>85,88</sup> For example, responsiveness towards isopropanol and toluene vapors has been demonstrated for a  $\text{TiO}_2$ - and  $\text{SiO}_2$ -based BS with rhombic-shaped



**Fig. 11** (a) Optical response and cross-section FE-SEM image of a 1DPC with a planar defect towards different partial pressures of isopropanol (left) and water (right) vapors, respectively. The arrows indicate the increase in the vapor partial pressure from 0 to 1; adapted and reprinted with permission from ref. 66, Copyright 2008 American Chemical Society. (b) 1DPC containing a nanophosphor layer as a defect and its response (luminescence (red) and reflectance (gray)) towards different partial pressures of isopropanol vapor: (i) before exposure (ii–v) at increasing partial pressure; adapted and reprinted with permission from ref. 88, Copyright 2010 Royal Society of Chemistry. (c) 1DPC with a defect layer comprised of dyed nanospheres embedded in a nanosheet layer shows increased response towards relative humidity when the dye is in the “turn-on” state (orange); adapted and reprinted with permission from ref. 85, Copyright 2017 John Wiley and Sons.

Eu-doped nanophosphors embedded in the middle of the structure (Fig. 11b).<sup>88</sup> In this case, the infiltration of the BS' voids with the analyte, and hence the optical response of the photonic structure towards a vapor, causes a strong modification of the luminescence spectrum of the nanophosphors. Note that the nanophosphors were embedded in a protective matrix to avoid interaction with the vapors. Upon increasing the partial vapor pressure, the average RI of the BS is increased due to adsorption and/or condensation of the high RI vapor in the pore walls, which results in a gradual red-shift of the resonant mode (Fig. 11b gray). Therefore, the intensity of the emission peak of the nanophosphor (Fig. 11b red) is slowly decreased because the match with the resonant mode is diminished. The higher the refractive index of the absorbed vapor, the larger the shift of the position of the resonant mode, which leads to a more abrupt drop of the emission peak intensity of the nanophosphor. Hence, this study showed that the luminescence spectra of the embedded nanophosphors are sensitive to the degree of matching with the resonant mode, and that the variations depend on the RI of the analyte, which implies selectivity of the response.

Additionally, the inclusion of a defect layer in a stimuli-responsive 1DPC opens up new possibilities in terms of readout scheme. For example, the integration of a light-emitting dye (polystyrene nanospheres dyed with Firefly Fluorescent Red) in the defect layer of a humidity-responsive PC (Fig. 11c) allows the creation of a tailored photoluminescence response to changes in ambient humidity.<sup>85</sup> Specifically,

antimony phosphate nanosheets were used as a stimuli-responsive defect layer in a TiO<sub>2</sub> and SiO<sub>2</sub>-based 1DPC, as they exhibit pronounced swelling upon exposure to humidity. When the nanosheet layer shows gradual swelling in response to increased humidity, the spatial and spectral positions of the reflectance dip are changed with respect to those of the emission band of the dye molecules. In this case two different scenarios can be realized, namely the *turn-on* or *turn-off* response of the luminescence of the dyes with increasing humidity. However, in the present state, the range of solvent vapors that has been detected with defect 1DPCs is still quite small.

### 6.3 Hybrid 1DPCs

A much wider range of applicable solvent vapors has been reported for hybrid 1DPCs, which combine the advantages of metal oxide NPs as RI contrast material, such as TiO<sub>2</sub> and SiO<sub>2</sub>, with materials that show response towards various analytes. As the library of responsive materials is vast, this opens up the opportunity to judiciously fine-tune the 1DPC to meet specific requirements, and the possibility to distinguish between different vapors. For example, 1DPCs comprised of TiO<sub>2</sub> NPs and MOFs are promising candidates for selective vapor sensing due to their modular tunability, strong host-guest interactions, and tailorable sorption behavior at the molecular level.<sup>62</sup> The first MOF-based 1DPC was reported by Hinterholzinger *et al.* and made use of ZIF-8 as active component.<sup>62</sup> The studied vapors included MeOH, EtOH, iso-butanol and *tert*-pentanol.

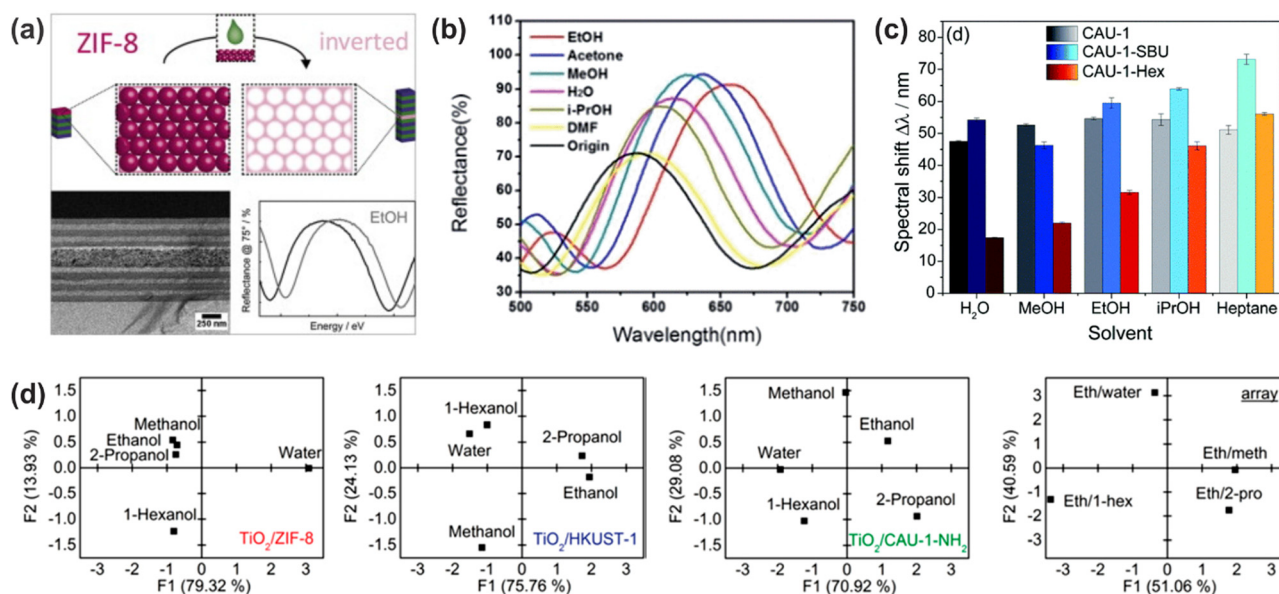


**Fig. 12** (a) Stimuli-responsive MOF defect layer incorporated in a 1DPC for enhanced sensitivity towards EtOH vapor; adapted and reprinted with permission from ref. 87, Copyright 2015 Elsevier. (b) Selective vapor sensing through a “breathing” MOF in the 1DPC; adapted and reprinted with permission from ref. 83, Copyright 2014 Royal Society of Chemistry. (c) Different spectral shifts upon analyte exposure for modified MOF building units in 1DPCs; adapted and reprinted with permission from ref. 113, Copyright 2018 Royal Society of Chemistry. (d) Principal component analysis (PCA) of 1DPCs for differently responsive MOF species (TiO<sub>2</sub>/ZIF-8, TiO<sub>2</sub>/HKUST-1, and TiO<sub>2</sub>/CAU-1-NH<sub>2</sub>) as active components and an array assembled from these three MOF-based BSs illustrating the combinatorial capability for discriminating between solvent vapor mixtures; adapted and reprinted with permission from ref. 63, Copyright 2015 American Chemical Society.



Later, the analyte-specific optical detection was enhanced by Ranft *et al.* by integrating multiple responsive MOF species (ZIF-8, CAU-1-NH<sub>2</sub>, HKUST-1) into a single 1DPC, whereby the response towards MeOH, EtOH, water, 2-propanol, 1-hexanol and mixtures was examined (Fig. 12d).<sup>63</sup> The analyte discrimination capability in CAU-1 based 1DPCs was enhanced by post-assembly modification of the coordination environment of the metal-oxo secondary building unit or by amide-formation at the organic linker, which translates into significant changes in the optical response of the photonic crystal sensor towards the analytes (Fig. 12c).<sup>113</sup> In this case, the used vapors were MeOH, EtOH, water, iso-propanol and heptane. As discussed in Section 5, a change in layer thickness upon exposure towards a stimulus leads to much larger optical shifts than a response based on RI changes. Therefore, the use of flexible MOFs such as NH<sub>2</sub>-MIL-88B, which show a pronounced “breathing effect” upon exposure to environmental vapors (MeOH, EtOH, water, iso-propanol, DMF, acetone and EtOH/water mixture), is beneficial for obtaining large optical shifts up to 200 nm (Fig. 12b).<sup>83</sup>

Even larger optical shifts in response to vapors have been obtained in hybrid 1DPCs built from metal-oxide NPs and nanosheets such as HSBP<sub>2</sub>O<sub>8</sub>, H<sub>3</sub>Sb<sub>3</sub>P<sub>2</sub>O<sub>14</sub> or Li<sub>2</sub>Sn<sub>2</sub>S<sub>5</sub> due to their pronounced swelling capability upon analyte exposure. Preceding work on the influence of relative humidity on the stacking distance of the layered bulk antimonyphosphates revealed that the phosphatoantimonic acids can intercalate a larger amount of water at ambient RH than their potassium counterparts.<sup>114</sup> Specifically, in the HSBP<sub>2</sub>O<sub>8</sub> bulk material proton diffusion behaves like a particle hydrate, while in the H<sub>3</sub>Sb<sub>3</sub>P<sub>2</sub>O<sub>14</sub>·*x* H<sub>2</sub>O bulk it behaves like a true lattice hydrate.<sup>114</sup> Inspired by this work, ellipsometric studies of the RH dependent swelling of these materials in nanosheet-based thin films were carried out.<sup>76</sup> These studies showed that in the thin film case the materials exhibit a smoother, less stepwise swelling upon exposure to RH compared to the bulk material, which is highly beneficial for application of this material in sensing. This effect can be attributed to a lower layer registry and less interlayer interactions in the restacked nanosheet material compared to the crystalline bulk material, and to increased grain boundary adsorption. Taking into account the turbostratic disorder of the nanosheets, the water adsorption sites between the nanosheets are less well-defined compared to the bulk, leading to a smoother, continuous water uptake rather than the formation of defined hydrates.<sup>76</sup> Inspired by the unprecedentedly large swelling capabilities of antimonyphosphate nanosheet thin films, paired with the fast sub-second to few seconds response times, 1DPCs with H<sub>3</sub>Sb<sub>3</sub>P<sub>2</sub>O<sub>14</sub> and either TiO<sub>2</sub> or SiO<sub>2</sub> were fabricated. In this case, the H<sub>3</sub>Sb<sub>3</sub>P<sub>2</sub>O<sub>14</sub> acts as the moisture-sensitive component while the nanoparticle layers are a “gate”, due to their textural porosity, providing access of the water molecules to the sensing component throughout the whole photonic structure.<sup>65,76</sup>

Even though HSBP<sub>2</sub>O<sub>8</sub> also exhibits extraordinary swelling capabilities, the main difference to H<sub>3</sub>Sb<sub>3</sub>P<sub>2</sub>O<sub>14</sub> is that it loses

water completely at zero humidity and therefore shows better contrast and thus superior sensitivity in the low humidity regime.<sup>75</sup> This behavior originates from the differences in the crystal structure of these materials. While H<sub>3</sub>Sb<sub>3</sub>P<sub>2</sub>O<sub>14</sub> exhibits structural pores that can host water molecules within the layers, the HSBP<sub>2</sub>O<sub>8</sub> layers are dense. A photonic nose based on HSBP<sub>2</sub>O<sub>8</sub> nanosheets and TiO<sub>2</sub> was developed (Fig. 13b), which allows trace water sensing and vapor recognition of alcohol/water mixtures, MeOH, EtOH, water, propanol, iso-propanol, butanol, 2-butanol, acetonitrile, toluene and heptane.<sup>75</sup> Hereby, the sensor can distinguish between water vapor, nonprotic (nonpolar and polar) and protic solvent vapors (alcohols) by exploiting the saturation time and optical shift as two independent descriptors. Even chemically similar solvent vapors such as homologous alcohols or isomers, which interact with the nanoparticle layers as well as the nanosheet layers of the 1DPC, can be distinguished based on their sorption and diffusion properties.<sup>75</sup>

Another interesting application is the exploitation of the giant moisture responsiveness of H<sub>3</sub>Sb<sub>3</sub>P<sub>2</sub>O<sub>14</sub> and TiO<sub>2</sub> or SiO<sub>2</sub> 1DPCs for touchless optical finger motion tracking (Fig. 13a) due to the fast intercalation of the humidity close to the finger into the nanosheet layers and the resulting optical shift.<sup>76</sup> In a recent publication, we demonstrated that this specific 1DPC could be transferred to arbitrary substrates (Fig. 13c) with the aid of a sacrificial layer without impairing the vapor sensing capability. In addition, it was shown that the sensing properties can be flexibly changed and fine-tuned through modification with various primary alkylamines.<sup>115</sup> Particularly, this allows to flexibly fine-tune the hydrophobicity of the sample and therefore the response towards VOCs.<sup>115</sup> Even though the fine-tuning of the sensing properties of 1DPCs has not received extensive attention so far, we believe that there is high potential for future research. As there is a wide variety of literature concerning intercalation in layered (nano)materials, this may open up the opportunity of judiciously creating stimuli-responsiveness and tunability in inherently non-responsive building blocks.

To the best of our knowledge, the highest reported RI contrast in 1DPCs was achieved in a hybrid BS which combined Li<sub>2</sub>Sn<sub>2</sub>S<sub>5</sub> nanosheets with SiO<sub>2</sub> nanoparticles.<sup>25</sup> In combination with the excellent swelling capability of the nanosheets upon exposure to humidity, this device bodes well for a new generation of humidity sensors with extremely high sensitivity.

In this chapter, we highlighted some vapor sensing applications of stimuli-responsive 1DPCs taking into account the different analytes that have been studied as well as the various materials that are suitable and different 1DPC architectures that are applicable. In terms of sensitivity, we anticipate that future research (not only in the field of vapor sensing) will focus on hybrid 1DPCs due to their often superior swellability or combination of sensing mechanisms, and thus larger optical shifts. In addition, unleashing new stimuli-responsive materials for sensor integration holds great potential due to the vast variety of building blocks, chemical properties and responsiveness.





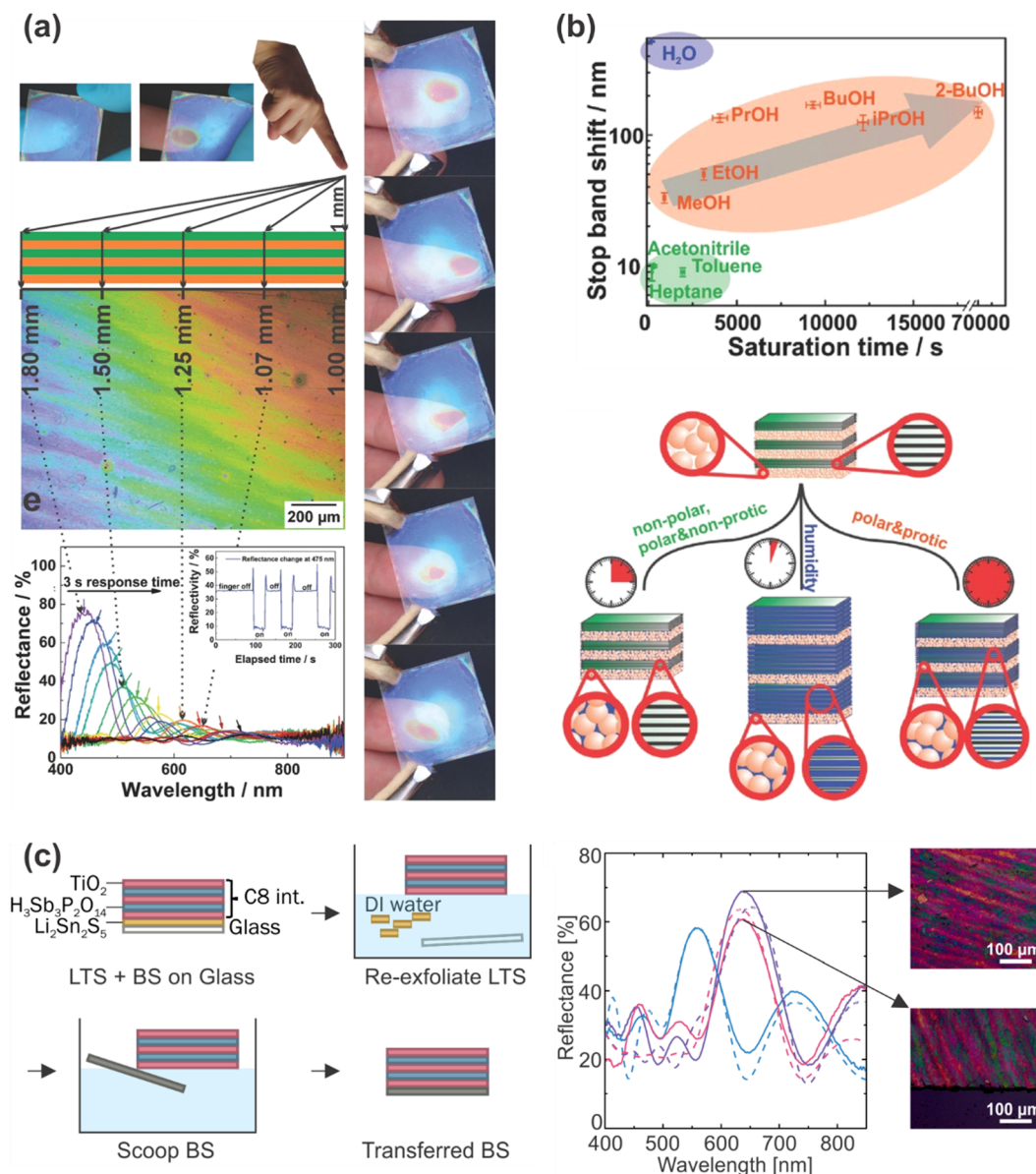


**Fig. 13** (a) 1DPC with giant moisture responsiveness used as a touchless positioning interface by responding to the moisture of a finger; adapted and reprinted with permission from ref. 76, Copyright 2015 John Wiley and Sons. (b) 1DPC acting as a photonic nose: analyte identification of different solvent vapors by different sensing mechanisms; adapted and reprinted with permission from ref. 75, Copyright 2016 John Wiley and Sons. (c) Left: Schematic description of the transfer of a vapor sensitive 1DPC to another substrate by hydrophobization of the sample (amine intercalation) and the use of a sacrificial layer. Right: Reflectance of the pristine (blue), hydrophobized (purple) and transferred (pink) sample along with the calculated reflectance (dashed lines) and microscope images of the sample before and after transfer; adapted and reprinted with permission from ref. 115, Copyright 2021 The Authors.

## 7 Current challenges of 1DPC sensors

Although many groups have focused on the architectures, techniques and materials in the field of 1DPC sensing, there are still several challenges limiting the performance of 1DPC-based sensors at the current state. These challenges emerge partly from the sensing field in general and are partly related specifically to 1DPCs.

For example, the miniaturization, which is highly desired for emerging application fields such as IoT, point of care testing, or

wearables, is an important aspect for both 1DPCs and the corresponding readout systems. While 1DPCs can easily be fabricated in small size, the miniaturization of the readout system remains challenging because quantitative measurements often rely on microscopic or spectroscopic techniques that require large and non-portable setups. A promising option to overcome this drawback is either the qualitative detection based on color changes induced through the sensing event, or building a readout platform that is based on handheld devices such as smartphones. By integrating the zoom function of the camera and systems for

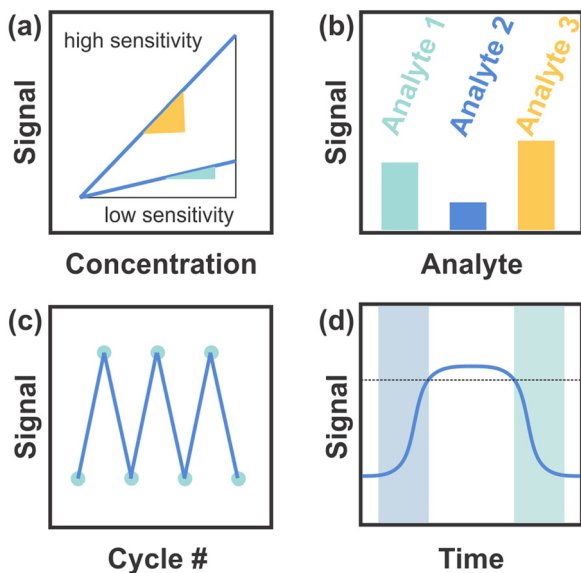


Fig. 14 (a) Sensitivity of the sensor based on the slope definition and the maximum sensitivity. (b) Selectivity of the sensor towards different analytes. (c) Stability of the sensor based on the number of cycles conducted. (d) Response (blue square) and recovery (green square) times. Figure adapted and reproduced from ref. 119.

optical analysis, colorimetric as well as fluorescence detection may be achieved thus rendering PCs a versatile sensing platform.<sup>116</sup>

Regarding the challenges specifically related to 1DPCs,<sup>90,117</sup> the key issues that need to be addressed to make them competitive with other sensor types are summarized schematically in Fig. 14. These parameters, also referred to as the “4S”, include the sensitivity (Fig. 14a), selectivity (Fig. 14b), stability (Fig. 14c) and speed (response-recovery rate; Fig. 14d).<sup>118</sup>

### 7.1 Sensitivity

In Fig. 14a the sensitivity – *i.e.* the measurement signal change per concentration unit of the analyte (slope definition) – is schematically depicted in accordance with the slope definition of the maximum sensitivity for a sensor with high (yellow) and low (green) sensitivity. Colorimetric 1DPC-based sensors that make use of RI changes as the main sensing mechanism often exhibit a stopband-shift of a few nanometers upon analyte infiltration at best, which makes a naked-eye-readout difficult. This can be improved with larger changes in the photonic stopband, *e.g.* by applying materials that show a large change in layer thickness, along with RI changes, in response to a stimulus. In these sensors, the sensitivity is enhanced and therefore future research should be directed in finding materials with pronounced swelling capability.

### 7.2 Selectivity

An example of the differentiating capability, and therefore the selectivity of a sensor towards different analytes, is given in Fig. 14b. A general issue in the field of sensing is the selectivity and cross sensitivity towards chemically similar analytes as the sensors are not labelled with recognition groups and often solely

distinguish different analytes by RI and polarity. This shortcoming can be alleviated by means of statistical data analysis, *e.g.* principal component analysis (PCA) of sensor arrays,<sup>4,63,67</sup> or hierarchical sensor structures.<sup>120</sup> The functionalization of the sensor with chemically selective recognition groups as well as the application of building blocks with inherent chemical selectivity might also help overcome this issue.

### 7.3 Stability

The sensor stability defines how long and throughout how many cycles the sensor maintains its performance, which is depicted schematically in Fig. 14c. Issues regarding the sensor stability include chemical stability, long-term stability and cyclability. For example, the sensor can undergo irreversible changes during the sensing event, or storage may affect the sensing performance, both of which is impracticable for long-term applications. Enhanced stability could be controlled, for example, by a careful choice of the building blocks (*i.e.* inorganic *vs.* organic materials) or morphology (*e.g.* active material with textural or structural porosity) of the sensor. Quite generally, the use of robust inorganic materials may lead to an improved chemical and long-term stability as compared to polymers.

### 7.4 Speed

Per definition, the speed of a sensor, *i.e.* the response and recovery times, is characterized by the times needed to achieve 90% of the signal change. This is illustrated in Fig. 14d, whereby the dotted line marks 90% of the signal change and the blue and green squares show the response and recovery times, respectively. As required by the desired application, swellable nanosheets with response times in the second to sub-second regime may be favored as functional building blocks for 1DPCs as compared to swellable polymers that typically exhibit response times in the range of up to several tens of minutes.

Lastly, the optimization of existing materials regarding the homogeneity of the particles (in terms of *e.g.* size, morphology, and phase purity), and the layer thicknesses as well as their surface roughness should be improved as these factors give rise to color purity and hence an improved color resolution of the sensor. This in turn facilitates the discrimination of analytes that only induce small shifts of the photonic stopband and may pave the way for continuous monitoring of physical, chemical or biochemical stimuli.

## 8 Summary and outlook

In this review, we have summarized the materials and principles for the design and fabrication of 1DPCs. The main fabrication methods rely on liquid processing and evaporation-induced self-assembly of the constituent materials without the need for expensive instrumentation or delicate processing conditions. Moreover, a large library of materials is available for the fabrication of 1DPCs including nanoparticles, polymers,



nanosheets, MOFs and zeolites. However, in order to transfer the materials and fabrication methods from research to industry, large-scale manufacturing needs to be improved tremendously. At the same time, the optical properties of PCs can be judiciously tuned based on theory-guided optical design. Hence, stimuli-responsiveness can be introduced rationally and translated into a visibly perceptible color change of the PC. Hereby, two different sensing mechanisms are possible based on the active component: change of RI or change of layer thickness. Since the RI changes are intrinsically limited, the use of 1DPC sensors that are based on layer thickness changes are favorable as the relative shift of the photonic stopband is more pronounced in this case. The main advantages of 1DPC sensors is their low cost and ease of readout. The response types can be divided into response towards physical or chemical stimuli, whereby we highlighted various examples of 1DPCs for each case. Furthermore, we introduced selected applications for 1DPCs in the field of vapor sensors, as we believe that this is a field with a bright future owing to the rapidly increased need for cheap and label-free sensor systems. In particular, different 1DPCs have been applied as “artificial noses” to detect humidity, explosives, toxic volatiles, or metabolic products. Finally, we provided an overview of several challenges that remain in 1DPC sensors, some of which stem from the sensing field in general and some of which are specific to 1DPCs.

Given the importance of sensors in our everyday life, photonic crystal based sensors represent a highly promising, low-cost technology for smart next-generation sensors, particularly regarding their subtle response to the environment for ambient monitoring and point-of-care applications. To achieve real-world applications in the near future it is of utmost importance to foster collaborative innovation from different research communities.

## Conflicts of interest

There are no conflicts to declare.

## Acknowledgements

Financial support was granted by the Max Planck Society, the University of Munich (LMU), the Center for Nanoscience and the Cluster of Excellence e-conversion. A. Jiménez-Solano gratefully acknowledges a postdoctoral scholarship from the Max Planck Society and the Spanish Ministry of Universities for funding through a Beatriz Galindo Research fellowship BG20/00015. Open Access funding provided by the Max Planck Society.

## References

- 1 X. Guo, D. Kuang, Z. Zhu, Y. Ding, L. Ge, Z. Wu, B. Du, C. Liang, G. Meng and Y. He, *ACS Appl. Nano Mater.*, 2021, **4**, 11159.
- 2 S. Su, W. Wu, J. Gao, J. Lu and C. Fan, *J. Mater. Chem.*, 2012, **22**, 18101.
- 3 F. Wang, Z. Meng, F. Xue, M. Xue, W. Lu, W. Chen, Q. Wang and Y. Wang, *Trends Environ. Anal. Chem.*, 2014, **3-4**, 1.
- 4 L. D. Bonifacio, G. A. Ozin and A. C. Arsenault, *Small*, 2011, **7**, 3153.
- 5 Y. Lu, S. Peng, D. Luo and A. Lal, *Nat. Commun.*, 2011, **2**, 578.
- 6 Y. Guo, M. Zhong, Z. Fang, P. Wan and G. Yu, *Nano Lett.*, 2019, **19**, 1143.
- 7 C. Liu, B. Zhang, W. Chen, W. Liu and S. Zhang, *TrAC, Trends Anal. Chem.*, 2021, **143**, 116334.
- 8 X. Wu, T. Chen, Y. Chen and G. Yang, *J. Mater. Chem. B*, 2020, **8**, 2650.
- 9 E. C. Nelson, N. L. Dias, K. P. Bassett, S. N. Dunham, V. Verma, M. Miyake, P. Wiltzius, J. A. Rogers, J. J. Coleman, X. Li and P. V. Braun, *Nat. Mater.*, 2011, **10**, 676.
- 10 R. A. Potyrailo, *Chem. Soc. Rev.*, 2017, **46**, 5311.
- 11 H. Ji, W. Zeng and Y. Li, *Nanoscale*, 2019, **11**, 22664.
- 12 U. Guth, W. Vonau and J. Zosel, *Meas. Sci. Technol.*, 2009, **20**, 042002.
- 13 X. Liu, S. Cheng, H. Liu, S. Hu, D. Zhang and H. Ning, *Sensors*, 2012, **12**, 9635.
- 14 S. H. Cho, J. M. Suh, T. H. Eom, T. Kim and H. W. Jang, *Electron. Mater. Lett.*, 2021, **17**, 1.
- 15 D.-H. Kim, J.-H. Cha, J. Y. Lim, J. Bae, W. Lee, K. R. Yoon, C. Kim, J.-S. Jang, W. Hwang and I.-D. Kim, *ACS Nano*, 2020, **14**, 16907.
- 16 T. Wang, Y. Guo, P. Wan, X. Sun, H. Zhang, Z. Yu and X. Chen, *Nanoscale*, 2017, **9**, 869.
- 17 X. Wang, Y. Li, X. Li, J. Yu, S. S. Al-Deyab and B. Ding, *Sens. Actuators, B*, 2014, **203**, 333.
- 18 J. Ge and Y. Yin, *Angew. Chem., Int. Ed.*, 2011, **50**, 1492.
- 19 Z. Cai, N. L. Smith, J.-T. Zhang and S. A. Asher, *Anal. Chem.*, 2015, **87**, 5013.
- 20 Z. Cai, X. Xu, Z. Meng, B. Rafique and R. Liu, *Functional Materials from Colloidal Self-Assembly*, 2022.
- 21 P. Ganter and B. V. Lotsch, *Mol. Syst. Des. Eng.*, 2019, **4**, 566.
- 22 S. G. J. J. D. Joannopoulos, J. N. Winn and R. D. Meade, *Photonic Crystals: molding the flow of light*, Princeton University Press, 2011.
- 23 M. E. Calvo and H. Míguez, *Responsive Photonic Nanostructures: Smart Nanoscale Optical Materials*, The Royal Society of Chemistry, 2013.
- 24 Y. Kang, J. J. Walish, T. Gorishnyy and E. L. Thomas, *Nat. Mater.*, 2007, **6**, 957.
- 25 K. Szendrei-Temesi, O. Sanchez-Sobrado, S. B. Betzler, K. M. Durner, T. Holzmann and B. V. Lotsch, *Adv. Funct. Mater.*, 2018, **28**, 1705740.
- 26 G. von Freymann, V. Kitaev, B. V. Lotsch and G. A. Ozin, *Chem. Soc. Rev.*, 2013, **42**, 2528.
- 27 A. Biswas, I. S. Bayer, A. S. Biris, T. Wang, E. Dervishi and F. Faupel, *Adv. Colloid Interface Sci.*, 2012, **170**, 2.
- 28 M. Qian, X. Q. Bao, L. W. Wang, X. Lu, J. Shao and X. S. Chen, *J. Cryst. Growth*, 2006, **292**, 347.
- 29 A. Altoukhov, J. Levrat, E. Feltin, J.-F. Carlin, A. Castiglia, R. Butté and N. Grandjean, *Appl. Phys. Lett.*, 2009, **95**, 191102.





- 30 G. A. Ozin, K. Hou, B. V. Lotsch, L. Cademartiri, D. P. Puzzo, F. Scotognella, A. Ghadimi and J. Thomson, *Mater. Today*, 2009, **12**, 12.
- 31 C. J. Brinker, Y. Lu, A. Sellinger and H. Fan, *Adv. Mater.*, 1999, **11**, 579.
- 32 S.-Y. Zhang, M. D. Regulacio and M.-Y. Han, *Chem. Soc. Rev.*, 2014, **43**, 2301.
- 33 C. Zhao, L. Xing, J. Xiang, L. Cui, J. Jiao, H. Sai, Z. Li and F. Li, *Particuology*, 2014, **17**, 66.
- 34 R. D. Deegan, O. Bakajin, T. F. Dupont, G. Huber, S. R. Nagel and T. A. Witten, *Nature*, 1997, **389**, 827.
- 35 A. Kaliyaraj Selva Kumar, Y. Zhang, D. Li and R. G. Compton, *Electrochem. Commun.*, 2020, **121**, 106867.
- 36 D. P. Puzzo, L. D. Bonifacio, J. Oreopoulos, C. M. Yip, I. Manners and G. A. Ozin, *J. Mater. Chem.*, 2009, **19**, 3500.
- 37 M. E. Calvo, O. Sánchez-Sobrado, S. Colodrero and H. Míguez, *Langmuir*, 2009, **25**, 2443.
- 38 T. Komikado, A. Inoue, K. Masuda, T. Ando and S. Umegaki, *Thin Solid Films*, 2007, **515**, 3887.
- 39 H. Shen, Z. Wang, Y. Wu and B. Yang, *RSC Adv.*, 2016, **6**, 4505.
- 40 J. Zhu and M. C. Hersam, *Adv. Mater.*, 2017, **29**, 1603895.
- 41 Z. Wu, D. Lee, M. F. Rubner and R. E. Cohen, *Small*, 2007, **3**, 1445.
- 42 A. Jiménez-Solano, J. F. Galisteo-López and H. Míguez, *Adv. Opt. Mater.*, 2018, **6**, 1700560.
- 43 C. Inui, Y. Tsuge, H. Kura, S. Fujihara, S. Shiratori and T. Sato, *Thin Solid Films*, 2008, **516**, 2454.
- 44 X. Yu, W. Ma and S. Zhang, *Dyes Pigm.*, 2021, **186**, 108961.
- 45 Z. Cai, Z. Li, S. Ravaine, M. He, Y. Song, Y. Yin, H. Zheng, J. Teng and A. Zhang, *Chem. Soc. Rev.*, 2021, **50**, 5898.
- 46 M. Barhoum, J. M. Morrill, D. Riassetto and M. H. Bartl, *Chem. Mater.*, 2011, **23**, 5177.
- 47 E. Yablonovitch, *Phys. Rev. Lett.*, 1987, **58**, 2059.
- 48 S. John, *Phys. Rev. Lett.*, 1987, **58**, 2486.
- 49 R. Srivastava, K. Thapa, S. Pati and S. Ojha, *Prog. Electromagn. Res. C*, 2008, **81**, 225.
- 50 J. C. Knight, *Nature*, 2003, **424**, 847.
- 51 H. Wang and K.-Q. Zhang, *Sensors*, 2013, **13**, 4192.
- 52 J. Zi, X. Yu, Y. Li, X. Hu, C. Xu, X. Wang, X. Liu and R. Fu, *Proc. Natl. Acad. Sci. U. S. A.*, 2003, **100**, 12576.
- 53 B. A. Bober, J. K. Ogata, V. E. Martinez, J. J. Hallinan, T. A. Leach and B. Negru, *J. Chem. Educ.*, 2018, **95**, 1004.
- 54 L. D. Bonifacio, B. V. Lotsch, D. P. Puzzo, F. Scotognella and G. A. Ozin, *Adv. Mater.*, 2009, **21**, 1641.
- 55 K. Tsakmakidis, *Nat. Mater.*, 2012, **11**, 1000.
- 56 D. A. G. Bruggeman, *Ann. Phys.*, 1935, **416**, 636.
- 57 J. C. M. Garnett and J. Larmor, *J. C. Philos. Trans. R. Soc.*, 1904, **203**, 385.
- 58 J. R. Link and M. J. Sailor, *Proc. Natl. Acad. Sci. U. S. A.*, 2003, **100**, 10607.
- 59 S. Y. Choi, M. Mamak, G. von Freymann, N. Chopra and G. A. Ozin, *Nano Lett.*, 2006, **6**, 2456.
- 60 J. Kobler, B. V. Lotsch, G. A. Ozin and T. Bein, *ACS Nano*, 2009, **3**, 1669.
- 61 B. Auguie, M. C. Fuertes, P. C. Angelomé, N. L. Abdala, G. J. A. A. Soler Illia and A. Fainstein, *ACS Photonics*, 2014, **1**, 775.
- 62 F. M. Hinterholzinger, A. Ranft, J. M. Feckl, B. Ruhle, T. Bein and B. V. Lotsch, *J. Mater. Chem.*, 2012, **22**, 10356.
- 63 A. Ranft, F. Niekil, I. Pavlichenko, N. Stock and B. V. Lotsch, *Chem. Mater.*, 2015, **27**, 1961.
- 64 K. Lazarova, H. Awala, S. Thomas, M. Vasileva, S. Mintova and T. Babeva, *Sensors*, 2014, **14**, 12207.
- 65 S. Colodrero, M. Ocaña and H. Míguez, *Langmuir*, 2008, **24**, 4430.
- 66 S. Colodrero, M. Ocana, A. R. Gonzalez-Elipe and H. Míguez, *Langmuir*, 2008, **24**, 9135.
- 67 L. D. Bonifacio, D. P. Puzzo, S. Breslav, B. M. Willey, A. McGeer and G. A. Ozin, *Adv. Mater.*, 2010, **22**, 1351.
- 68 M. M. Orosco, C. Pacholski, G. M. Miskelly and M. J. Sailor, *Adv. Mater.*, 2006, **18**, 1393.
- 69 G. M. Paternò, G. Manfredi, F. Scotognella and G. Lanzani, *APL Photonics*, 2020, **5**, 080901.
- 70 Z. Wang, J. Zhang, J. Li, J. Xie, Y. Li, S. Liang, Z. Tian, C. Li, Z. Wang, T. Wang, H. Zhang and B. Yang, *J. Mater. Chem.*, 2011, **21**, 1264.
- 71 Z. Wang, J. Zhang, J. Xie, C. Li, Y. Li, S. Liang, Z. Tian, T. Wang, H. Zhang, H. Li, W. Xu and B. Yang, *Adv. Funct. Mater.*, 2010, **20**, 3784.
- 72 K. Lazarova, R. Georgiev, M. Vasileva, B. Georgieva, M. Spassova, N. Malinowski and T. Babeva, *Opt. Quantum Electron.*, 2016, **48**, 310.
- 73 D. Kou, W. Ma, S. Zhang and B. Tang, *ACS Appl. Polym. Mater.*, 2020, **2**, 2.
- 74 E. Tian, J. Wang, Y. Zheng, Y. Song, L. Jiang and D. Zhu, *J. Mater. Chem.*, 2008, **18**, 1116.
- 75 P. Ganter, K. Szendrei and B. V. Lotsch, *Adv. Mater.*, 2016, **28**, 7436.
- 76 K. Szendrei, P. Ganter, O. Sánchez-Sobrado, R. Eger, A. Kuhn and B. V. Lotsch, *Adv. Mater.*, 2015, **27**, 6341.
- 77 K. Szendrei-Temesi, A. Jiménez-Solano and B. V. Lotsch, *Adv. Mater.*, 2018, **30**, 6289.
- 78 C. Yao, J. Zhao, H. Ge, J. Ren, T. Yin, Y. Zhu and L. Ge, *Colloids Surf., A*, 2014, **452**, 89.
- 79 C. Yao, J. Ren, C. Liu, T. Yin, Y. Zhu and L. Ge, *ACS Appl. Mater. Interfaces*, 2014, **6**, 16727.
- 80 J. Han, Y. Dou, M. Wei, D. G. Evans and X. Duan, *RSC Adv.*, 2012, **2**, 10488.
- 81 B. V. Lotsch and G. A. Ozin, *Adv. Mater.*, 2008, **20**, 4079.
- 82 B. V. Lotsch and G. A. Ozin, *ACS Nano*, 2008, **2**, 2065.
- 83 Z. Hu, C.-a. Tao, F. Wang, X. Zou and J. Wang, *J. Mater. Chem. C*, 2015, **3**, 211.
- 84 M. C. Fuertes, F. J. López-Alcaraz, M. C. Marchi, H. E. Troiani, V. Luca, H. Míguez and G. J. A. A. Soler-Illia, *Adv. Funct. Mater.*, 2007, **17**, 1247.
- 85 K. Szendrei, A. Jiménez-Solano, G. Lozano, B. V. Lotsch and H. Míguez, *Adv. Opt. Mater.*, 2017, **5**, 1700663.
- 86 O. Sánchez-Sobrado, G. Lozano, M. E. Calvo, A. Sánchez-Iglesias, L. M. Liz-Marzán and H. Míguez, *Adv. Mater.*, 2011, **23**, 2108.



- 87 A. Ranft, I. Pavlichenko, K. Szendrei, P. M. Zehetmaier, Y. Hu, A. von Mankowski and B. V. Lotsch, *Microporous Mesoporous Mater.*, 2015, **216**, 216.
- 88 O. Sanchez-Sobrado, M. E. Calvo, N. Nunez, M. Ocana, G. Lozano and H. Míguez, *Nanoscale*, 2010, **2**, 936.
- 89 J. Ren, H. Xuan, C. Liu, C. Yao, Y. Zhu, X. Liu and L. Ge, *RSC Adv.*, 2015, **5**, 77211.
- 90 C. Fenzl, T. Hirsch and O. S. Wolfbeis, *Angew. Chem., Int. Ed.*, 2014, **53**, 3318.
- 91 M. Kolle, B. Zheng, N. Gibbons, J. J. Baumberg and U. Steiner, *Opt. Express*, 2010, **18**, 4356.
- 92 Y. Lu, H. Xia, G. Zhang and C. Wu, *J. Mater. Chem.*, 2009, **19**, 5952.
- 93 H. Ma, M. Zhu, W. Luo, W. Li, K. Fang, F. Mou and J. Guan, *J. Mater. Chem. C*, 2015, **3**, 2848.
- 94 A. C. Arsenault, T. J. Clark, G. von Freymann, L. Cademartiri, R. Sapienza, J. Bertolotti, E. Vekris, S. Wong, V. Kitaev, I. Manners, R. Z. Wang, S. John, D. Wiersma and G. A. Ozin, *Nat. Mater.*, 2006, **5**, 179.
- 95 Y. Yue and J. P. Gong, *J. Photochem. Photobiol., C*, 2015, **23**, 45.
- 96 E. P. Chan, J. J. Walish, E. L. Thomas and C. M. Stafford, *Adv. Mater.*, 2011, **23**, 4702.
- 97 S. Zhou and C. Wu, *Macromolecules*, 1996, **29**, 4998.
- 98 M. Li and J. Bae, *Polym. Chem.*, 2020, **11**, 2332.
- 99 M. C. Chiappelli and R. C. Hayward, *Adv. Mater.*, 2012, **24**, 6100.
- 100 R. Ozaki, T. Matsui, M. Ozaki and K. Yoshino, *Jpn. J. Appl. Phys.*, 2002, **41**, L1482.
- 101 K. Hwang, D. Kwak, C. Kang, D. Kim, Y. Ahn and Y. Kang, *Angew. Chem., Int. Ed.*, 2011, **50**, 6311.
- 102 I. Pavlichenko, A. T. Exner, M. Guehl, P. Lugli, G. Scarpa and B. V. Lotsch, *J. Phys. Chem. C*, 2011, **116**, 298.
- 103 C. Liu, C. Yao, Y. Zhu, J. Ren and L. Ge, *Sens. Actuators, B*, 2015, **220**, 227.
- 104 Z. Wang, J. Zhang, Z. Wang, H. Shen, J. Xie, Y. Li, L. Lin and B. Yang, *J. Mater. Chem. C*, 2013, **1**, 977.
- 105 D. Kou, S. Zhang, J. L. Lutkenhaus, L. Wang, B. Tang and W. Ma, *J. Mater. Chem. C*, 2018, **6**, 2704.
- 106 B. V. Lotsch and G. A. Ozin, *J. Am. Chem. Soc.*, 2008, **130**, 15252.
- 107 B. V. Lotsch, F. Scotognella, K. Moeller, T. Bein and G. A. Ozin, Proc. SPIE 7713, Photonic Crystal Materials and Devices IX, 2010, 77130V.
- 108 Z. Wang, J. Zhang, Z. Tian, Z. Wang, Y. Li, S. Liang, L. Cui, L. Zhang, H. Zhang and B. Yang, *Chem. Commun.*, 2010, **46**, 8636.
- 109 G. Soler-Illia, M. Fuertes, P. Angelomé, M. Marchi, H. E. Troiani, V. Luca and H. Míguez, *Mesoporous multilayer thin films: photonic crystals sensitive to the environment*, 2008.
- 110 N. Hidalgo, M. E. Calvo and H. Míguez, *Small*, 2009, **5**, 2309.
- 111 O. Sanchez-Sobrado, M. E. Calvo and H. Míguez, *J. Mater. Chem.*, 2010, **20**, 8240.
- 112 R. A. Allardyce, V. S. Langford, A. L. Hill and D. R. Murdoch, *J. Microbiol. Methods*, 2006, **65**, 361.
- 113 A. von Mankowski, K. Szendrei-Temesi, C. Koschnick and B. V. Lotsch, *Nanoscale Horiz.*, 2018, **3**, 383.
- 114 S. Deniard-Courant, Y. Piffard, P. Barboux and J. Livage, *Solid State Ion.*, 1988, **27**, 189.
- 115 M. Däntl, S. Guderley, K. Szendrei-Temesi, D. Chatzitheodoridou, P. Ganter, A. Jiménez-Solano and B. V. Lotsch, *Small*, 2021, **17**, 2007864.
- 116 J. Hou, M. Li and Y. Song, *Angew. Chem., Int. Ed.*, 2018, **57**, 2544.
- 117 K. Szendrei-Temesi, PhD thesis, LMU Munich, 2018.
- 118 J. Zhang, X. Liu, G. Neri and N. Pinna, *Adv. Mater.*, 2016, **28**, 795.
- 119 P. Ganter, PhD thesis, LMU Munich, 2018.
- 120 T. L. Kelly, A. Garcia Segal and M. J. Sailor, *Nano Lett.*, 2011, **11**, 3169.

